



City Research Online

City St George's, University of London

Citation: Qian, K., Liang, S-L., Xiong, X-Y., Fu, F. & Fang, Q. (2020). Quasi-Static and Dynamic Behavior of Precast Concrete Frames with High Performance Dry Connections subjected to Loss of a Penultimate Column Scenario. *Engineering Structures*, 205, 110115. doi: 10.1016/j.engstruct.2019.110115

This is the accepted version of the paper.

This version of the publication may differ from the final published version. To cite this item please consult the publisher's version.

Permanent repository link: <https://openaccess.city.ac.uk/id/eprint/23392/>

Link to published version: <https://doi.org/10.1016/j.engstruct.2019.110115>

Copyright and Reuse: Copyright and Moral Rights remain with the author(s) and/or copyright holders. Copies of full items can be used for personal research or study, educational, or not-for-profit purposes without prior permission or charge, unless otherwise indicated, provided that the authors, title and full bibliographic details are credited, a hyperlink and/or URL is given for the original metadata page and the content is not changed in any way. For full details of reuse please refer to [City Research Online policy](#).

27 **Keywords:** Dynamic, Static and Progressive Collapse; Precast Concrete; Unbonded Posttensioned
28 Analysis

29 * Corresponding author. Tel.: 86+771-3232894, E-mail address: qiankai@gxu.edu.cn

30 **1. Introduction**

31 Unbonded post-tensioned precast concrete (UPPC) system was first advocated in PREcast
32 Seismic Structural System (PRESSSS) program [1] due to its high-ability of self-centering and low
33 residual deformation. Afterwards, a number of studies have been carried out to further investigate its
34 seismic performance of UPPC system. To enhance the energy dissipation ability of UPPC system,
35 Stone et al. [2] and Stanton et al. [3] embedded mild steel across the beam-column joints. However,
36 this modification may lead to irreparable damage at the beam ends causing certain difficulties in
37 construction. Therefore, extensive studies [4-10] were devoted to facilitate the reparability of the
38 UPPC system.

39 Previous studies indicated that UPPC system performed well under cyclic loads. Different to
40 seismic design, progressive collapse design focused on gravity load redistribution capacity of the
41 structures. Moreover, the ability of developing secondary load resisting mechanism to mitigate
42 progressive collapse requires sufficient deformation capacity and ductility. However, investigation
43 on progressive collapse performance of UPPC system is rare. Lu et al. [11] proposed a sort of
44 unbonded posttensioned steel-concrete composite frame for seismic and progressive collapse
45 mitigation. The proposed frame exhibited better behavior than conventional frames in resisting
46 either seismic loading or progressive collapse. Qian et al. [12] experimentally investigated the
47 performance of UPPC frames with different dry connections to resist progressive collapse. They
48 reported that compressive arch action (CAA) and tensile catenary action (TCA) could be mobilized
49 to resist progressive collapse simultaneously. However, only quasi-static behavior was investigated
50 and the dynamic response of UPPC frame under sudden removal of a penultimate column, which
51 representing a typical terrorist attack or vehicular impact scenario, was in need of investigation.

52 As it is stipulated in DoD [13], four methods for progressive collapse analysis: linear static (LS),
53 nonlinear static (NS), linear dynamic (LD), and nonlinear dynamic (ND) analyses can be used for
54 progressive collapse design. LS and NS analyses are easy to perform while they fall short in
55 capturing dynamic nature of progressive collapse. LD analysis is capable of including inertia effects
56 while fail to account for nonlinear characteristic of the building. Therefore, ND analysis is the best
57 option for progressive collapse analysis due to its high accuracy. However, ND analysis requires
58 substantial computing resource which results in inconvenience in engineering application. To
59 integrate advantages, load increase factor (LIF) and dynamic increase factor (DIF) are proposed to
60 convert LS results and NS results to ND behavior, respectively. Relying on this, dynamic resistance
61 could be obtained from quasi-static response. Considerable efforts have been carried out to
62 investigate the nonlinear static response of beam-column sub-assemblages under column removal
63 scenario through quasi-static tests. Sadek et al. [14] tested two full scaled reinforced concrete (RC)
64 assemblies in accordance with different seismic intensity. In their tests, the decline of load
65 resistance was measured due to concrete crushing while re-ascending of load resistance was
66 observed owing to TCA. Moreover, the failure of the assemblies was controlled by fractured of
67 bottom rebar near the middle column. Qian and Li [15-16] performed a series of tests to study the
68 load redistribution capacity of RC frame subjected to the loss of a corner column. They reported that
69 CAA and TCA were inefficient due to limited axial restraints. Yu and Tan [17] investigated the
70 structural behavior of RC beam-column sub-assemblages under a middle column removal scenario.
71 It was found that both CAA and TCA could be developed as long as adequate axial and rotational
72 restraints provided. Valipour et al. [18] studied the effects of concrete strength and reinforcement
73 ratio on behavior of RC frames to mitigate progressive collapse. The test results indicated that the
74 relationship between CAA capacity and concrete strength is approximately linear whereas
75 reinforcement ratio has a minor effect on the contribution of CAA. Quiel et al. [19] proposed a new
76 type of connection for precast concrete buildings to resist progressive collapse, the connection
77 exhibited favorable damage avoidance capacity. Meanwhile, several dynamic tests were also
78 performed recently. Qian and Li [20-21] evaluated the dynamic performance of RC frame under the

79 loss of a corner column by using specially designed column removal apparatus. Furthermore, DIF
80 was quantified by comparing the dynamic response to corresponding static one. They proposed that
81 the DIF recommended by DoD [13] for structural component with force-controlled behavior may be
82 too conservative. Yu et al. [22] reported the dynamic progressive collapse response of RC sub-
83 assemblages under an explosively removed column. The test results proved that the strain effects of
84 material were insignificant. Russell et al. [23] performed static and dynamic tests to investigate the
85 load carrying capacity of RC flat structure under different column removal scenarios (corner,
86 penultimate or interior column). They found that the load distribution behavior obtained from
87 dynamic tests was similar to that from static ones. They also proposed that the recommended DIF
88 was conservative. Qian et al. [24] experimentally and numerically investigated the dynamic
89 behavior of RC flat slab structure under two column missing scenario. The results indicated that RC
90 flat slab structure could achieve new balance even two columns (one interior and one side column)
91 were removed suddenly.

92 In addition, energy equivalent method [25] is frequently used to assess the dynamic response
93 based on measured quasi-static load resisting function. However, this method ignores the effects of
94 damping and thus may lead to conservative prediction. Single-degree-of-freedom (SDOF) model [26-
95 28] is another favorable way to predict dynamic response. After conducting dynamic incremental
96 analysis, the dynamic ultimate load (DUL) of the specimens can be obtained and therefore a force
97 based DIF, which is defined as the ratio of static ultimate load (SUL) to the DUL, can be obtained
98 [20].

99 To have a deeper understanding of the difference of static procedure and dynamic procedure
100 stipulated in the design codes, in this paper, two UPPC frames were designed and tested under quasi-
101 static test regime to investigate the load resisting mechanism of UPPC system subjected to the loss of
102 a penultimate column scenario. Meanwhile, two counterparts, which have identical reinforcement
103 details and dimensions, were tested under dynamic test regime using specially designed column
104 removal apparatus to capture their dynamic response subjected to sudden column missing scenarios.
105 Note that, the DUL could not be determined purely relied on these two dynamic tests. For this reason,

106 a SDOF model was developed based on the response captured from quasi-static tests. After validation,
107 the proposed model was employed to determine the DUL of tested dynamic specimens. Moreover,
108 the model was used to investigate the effect of service load, non-zero initial condition, and damping
109 ratio on dynamic response caused by sudden column missing.

110 **2. Experimental program**

111 2.1. Test specimens

112 In this study, four 1/2 scaled UPPC beam-column substructures, extracted from the prototype
113 structure at the inflection points, were tested subjected to either quasi-static or dynamic loading
114 regimes. The prototype structure is an eight-storey frame located on a D class site, which was
115 designed in accordance with ACI 318-14 [29]. The design response spectrum acceleration parameters
116 of SDS and SD1 are 0.46 and 0.29, respectively. The design live load (LL) is 2.0 kPa. The dead load
117 (DL) including the ceiling weight is 5.1 kPa. Table 1 tabulates the characteristics of the specimens.
118 These four specimens can be categorized into two groups (UPPC-S and UPPC-D). The quasi-static
119 group includes UPPC-SL and UPPC-SH whereas the dynamic group has two specimens UPPC-DL
120 and UPPC-DH. The designation “UPPC” represents Unbonded Posttensioned Precast Concrete
121 frame. The letter “S” and “D” represent quasi-static and dynamic test, respectively. In addition, the
122 last letter “L” and “H” denote axial compression ratio of 0.2 and 0.4 at the side column, respectively.
123 It should be noted that all specimens have identical reinforcement detailing and dimensions. As
124 shown in Fig. 1, the specimen consists of two beams, two side columns, one middle column stub, and
125 an overhanging beam beyond one of the side columns as a penultimate column removal was
126 assumed. The side column with overhanging beam represents interior side column (to simulate
127 horizontal restraints from surrounding bays). Conversely, the side column without overhanging
128 beam represents exterior side column where no additional horizontal restraints.

129 The cross-section of beam and column was 150 mm × 250 mm and 250 mm × 250 mm,
130 respectively. The longitudinal reinforcement for column is 4T16 while the top and bottom beam were
131 both 2T12. R6 was used as transverse reinforcements for beam and column. “T16”, “T12”, and “R6”

132 represent deformed rebar with diameter of 16 mm, 12 mm, and plain rebar with diameter of 6 mm,
133 respectively. Moreover, spiral hoops with diameter of 60 mm were embedded at the beam ends to
134 enhance the concrete strength. PVC tubes with diameter of 20 mm were embedded in the precast
135 beams and columns for assembly purpose. The beams and columns were assembled by unbonded
136 posttensioned strands with nominal diameter and area of 12.7 mm and 98.7 mm², respectively.

137 2.2. Material properties

138 At the day of tests, cylinder tests indicated, the concrete compressive strength of UPPC-SL,
139 UPPC-SH, UPPC-DL, and UPPC-DH, were 38.5 MPa, 39.4 MPa, 37.5 MPa, and 38.1 MPa,
140 respectively. In addition, the tensile splitting tests indicated the tensile strength at the day of test is
141 3.7 MPa, 3.6 MPa, 3.5 MPa, and 3.8 MPa, for UPPC-SL, UPPC-SH, UPPC-DL, and UPPC-DH,
142 respectively. The properties of the reinforcements and strands were listed in Table 2.

143 2.3. Test setup and instrumentations

144 Fig. 2 gives test setup and layout of instrumentations. For quasi-static tests, as shown in Fig. 2a,
145 the top of side column and overhanging beam, if any, were connected to an A-frame via a roller
146 connection while the bottom of the side column was sit on a pin support. The ground level
147 penultimate column was removed prior to vertical load applied by a hydraulic jack (Item 1 in Fig.
148 2a). To prevent undesired out-of-plane failure, a steel assembly (Item 3 in Fig. 2a) was specially
149 placed beneath the hydraulic jack (Item 1 in Fig. 2a). The axial compressive force on the side column
150 was applied by a hydraulic jack (Item 6 in Fig. 2a) with a self-equilibrium system. To measure test
151 results properly, extensive instrumentations were installed. A load cell (Item 2 in Fig. 2a) was
152 installed just below the hydraulic jack (Item 1 in Fig. 2a) to measure the applied concentrated load.
153 Tension/compression load cell (Item 5 in Fig. 2a) was installed at each roller to measure the
154 horizontal reaction force of the roller. A load pin (Item 8 in Fig. 2a) was installed at the pin support
155 to measure the vertical and horizontal reaction force of the pin support. Therefore, the behavior of
156 vertical load redistribution and the varying of horizontal reaction force were monitored during test.
157 Moreover, to monitor the varying of prestressing force of the strand, a load cell (Item 4 in Fig. 2a)

158 was installed at the jacking end for each strand. Furthermore, a series of linear variable differential
159 transformers (LVDTs) were installed along the beam span and column height to monitor the
160 deformation shape of the beams and columns.

161 For dynamic tests, as shown in Fig. 2b, the test setup of dynamic specimens is almost similar to
162 that of quasi static one, except the ground penultimate column was replaced by a specially designed
163 sudden column removal device (SCRD, Item 10 in Fig. 2b). The SCRD comprised a steel column, a
164 pin support, and a load cell, which had been used in [20]. Then, six weight blocks (Item 9 in Fig. 2b)
165 with total weights of 8400 kg, were hung along the beam to simulate the service load
166 ($2(1.2DL+0.5LL)$) required by load combination of dynamic analysis procedure stipulated by DoD
167 [13]. After that, the SCRD was suddenly removed to replicate the sudden column removal. To
168 monitor the variation of axial force in SCRD, a load cell (Item 11 in Fig. 2b) was installed beneath
169 the steel column of the SCRD. Similar to static tests, the axial force of the roller and the vertical and
170 horizontal reaction force of the pin supports and prestressing force of the strands were also measured
171 in the dynamic tests, as shown in Fig. 2c.

172 **3. Quasi-Static test observation and results**

173 To facilitate readability, the nomenclature of this paper is shown in Table 3. As mentioned above,
174 UPPC-SL and UPPC-SH were tested under quasi-static push-down loading regime. The key results
175 such as first peak load (FPL), second peak load (SPL) and maximum horizontal compressive/tensile
176 force on the exterior and interior side (E-MHCF/E-MHTF, I-MHCF/I-MHTF) were summarized in
177 Table 4.

178 *3.1. Global behavior and failure modes*

179 Fig. 3 gives the load-middle joint displacement (MJD) curve of the specimens. The FPL of
180 UPPC-SL and UPPC-SH is 39 kN and 41 kN, respectively. At relatively small deformation stage, the
181 initial stiffness of UPPC-SH is slightly higher than that of UPPC-SL as the higher axial compressive
182 ratio on side column increases the stiffness of horizontal restraints of the beams. The load resistance
183 of UPPC-SH is greater than that of UPPC-SL until the MJD reached 530 mm. It should be pointed

184 out that UPPC-SH reaches its SPL at MJD of 461 mm while UPPC-SL keeps increasing until
185 reaching an MJD of 600 mm. The SPL of UPPC-SH and UPPC-SL is 78 kN and 90 kN, respectively.
186 Therefore, larger compressive axial force on side column could increase its FPL and initial stiffness
187 slightly, but decrease its SPL and deformation capacity significantly, which could be explained as the
188 larger axial compressive force on side column resulted in the failure of side column earlier due to
189 greater $P-\Delta$ effects in exterior side column.

190 Fig. 4 presents the failure modes of UPPC-SL. As shown in the figure, wide openings were
191 observed at the beam-column interfaces. The damage of beam was concentrated at compressive toes
192 while no cracks are observed along the beams during the test as the unbonded posttensioned strands
193 induces considerable compressive stress and the beam longitudinal reinforcement is discontinuous at
194 the beam-column interface. At the end of the test, the exterior side column (without overhanging
195 beam) experiences a typical large eccentric compression failure. However, the interior side column is
196 observed much milder damage: only few flexural cracks formed in the inner face of the side column.
197 This is because the overhanging beam could provide required horizontal restraints and resulting in
198 less $P-\Delta$ effects. In general, as shown in Fig. 5, similar phenomenon is observed for UPPC-SH.
199 Compared to UPPC-SL, the concrete crushing of exterior side column of UPPC-SH is more severe
200 due to greater $P-\Delta$ effects. The observation above proves that the failure modes of UPPC frames are
201 quite different from that of RC frames [14-15, 17, 30-31] and commonly used precast concrete
202 frames with wet or dry connections [32-35]. In these tests, plastic hinges are formed at the beam ends
203 and penetrated cracks were formed along the beam at catenary action stage.

204 3.2. *Deformation shape of the beam and column*

205 Fig. 6 presents the varying of deformation shape of the double-bay beam of UPPC-SL in
206 accordance with different MJDs. It can be found that the double-bay beams deformed in a twofold
207 line manner during the test, which agrees well with the failure mode. Generally, similar results are
208 measured at UPPC-SH. Fig. 7 illustrates the lateral deflection of the side column of UPPC-SH. The
209 lateral displacement achieved negative (outward) first and then changes to positive (inward). For the

210 exterior side column, the maximum outward and inward movements are -0.69 mm and 43.43 mm,
211 respectively. However, they are -0.62 mm and 7.6 mm for interior side column, respectively.

212 3.3. Horizontal reaction force

213 Figs. 8a and b illustrate the distribution of horizontal reaction of UPPC-SH on exterior and
214 interior side, respectively. Due to horizontal restraint, the outward and inward movement causes
215 compressive (negative value) and tensile (positive value) reaction on the boundary. It can be found
216 that column bottom restraint contributes majority of compressive reaction force on both sides
217 whereas the contribution from top roller could be ignored maybe due to relatively large gap existed.
218 With increased displacement, the horizontal reaction force changes from compression to tension
219 following increased prestressing forces in strands. In tension phase, column top and bottom provide
220 tensile reaction force almost equally for exterior side. However, the roller connected to the
221 overhanging beam contributes majority of tensile reaction force for interior side column. Generally,
222 similar phenomenon is measured at UPPC-SL. Table 4 tabulates the maximum horizontal reaction of
223 the specimens. For UPPC-SL, the E-MHCF, I-MHCF, E-MHTF, and I-MHTF are -62 kN, -75 kN,
224 135 kN and 259 kN, respectively. However, they are -67 kN, -84 kN, 156 kN, and 253 kN for UPPC-
225 SH, respectively. It proves that the interior side experiences larger reaction in both tension and
226 compression phase due to stronger restraints.

227 3.4. Bending moment in the exterior side column

228 To further reveal the failure mode of exterior side column, the variation of bending moment of the
229 exterior side column was illustrated in Fig. 9. As shown in the inserted figure, the bending moment in
230 section E-E can be determined by Eq. 1:

$$231 \quad M_E = H_l l_0 + V_l \Delta \quad (1)$$

232 where H_l is the horizontal reaction force from top roller; l_0 is the distance from top roller to
233 section E-E; V_l is the axial compressive force on the exterior side column; Δ is horizontal drift in
234 section E-E.

235 As shown in Fig. 9, the bending moment is negative at small deformation stage due to
236 compressive horizontal reaction force from top roller, whereas it changes to positive at large
237 deformation stage because the horizontal reaction force changes from negative to positive. Fig. 10
238 gives the theoretical bending moment-axial force curve of E-E section and the points represent the
239 measured axial force and maximum bending moment of the section. As the points located at the
240 portion of tensile failure, it agrees with the failure mode of the exterior side column well (large
241 eccentric compressive failure).

242 3.5. Load resisting mechanism

243 Due to special configuration, the load resisting mechanisms mobilized in UPPC frame are
244 significantly different to that in RC frames [12]. For RC frames, flexural action (FA), CAA and TCA
245 will be mobilized in sequence to mitigate collapse. For UPPC frames, as illustrated in Fig. 11, FA
246 will not develop due to limited rotational restraint at the beam end. CAA relies on the arching force
247 (N in the figure) in beam which is induced by prestressing force in the strands and axial restraint.
248 Moreover, the TCA due to tensioning of the strands is mobilized from the beginning of the test. Thus,
249 the TCA and CAA provide load carrying resistance simultaneously for UPPC frames. As the strands
250 are unbonded, the TCA is dominant by the vertical component of prestressing forces. The
251 contribution from CAA can be simply determined by subtracting the resistance of TCA from the
252 measured load resistance. Fig. 12 illustrates the decomposition of the load resistance. It can be found
253 that the CAA can even lead to negative contribution when MJD beyond one beam depth as the
254 direction of vertical component of the arching force changes from upward to downward (refer to Fig.
255 11b) when the MJD is larger than one beam depth. For conventional RC frames, the TCA due to
256 stretching of longitudinal reinforcements kicks in after vanish of CAA due to concrete crushing.

257 4. Dynamic test results

258 As mentioned above, to fully understand the dynamic response of UPPC frames subjected to
259 sudden column removal and compare the static and dynamic behavior of UPPC frames, two dynamic
260 specimens: UPPC-DL and UPPC-DH were dynamically tested under sudden column removal

261 scenario. As mentioned above, a total of about 8400 kg weights (steel assemblies) were hung below
262 the double-span beam before removal of the SCRD. As a result, an initial axial force of 40.5 kN and
263 40.2 kN were measured at the SCRD for UPPC-DL and UPPC-DH, respectively. The key results
264 such as the maximum middle joint displacement and maximum horizontal compressive/tensile force
265 were tabulated in Table 4. More detail discussion on dynamic response could be found as below.

266 4.1. Reliability of SCRD

267 To capture realistic dynamic response, the duration of column removal must be less than 10 % of
268 the natural period of the vibration of the remaining frame [13]. Fig. 13 gives the varying of axial
269 force in SCRD. As shown in the figure, for UPPC-DL, the initial axial force was 40.5 kN before
270 column removal at a time of 0.01 s and it reduced to 0.0 kN at a time of 0.018 s. Thus, the duration
271 was 0.008 s, which is about 1.1 % of its natural period of vibration. Similarly, the duration of UPPC-
272 DH was 0.005 s, which is about 0.9 % of its natural period. Thus, the reliability of the SCRD was
273 ensured.

274 4.2. Dynamic displacement responses

275 Figs. 14a and b illustrate the displacement response of UPPC-DL and UPPC-DH, respectively.
276 For UPPC-DL, the maximum MJD is 320 mm at a time of 2.1 s. The maximum displacement of
277 VD1, VD2, VD3, VD4, VD5, and VD6 are 88 mm, 170 mm, 253 mm, 250 mm, 168 mm, and 86
278 mm, respectively. For UPPC-DH, the maximum MJD is 295 mm a time of 1.99 s. The maximum
279 displacement of VD1, VD2, VD3, VD4, VD5, and VD6 are 76 mm, 160 mm, 235 mm, 230 mm, 153
280 mm, and 73 mm, respectively. The deformation shape of the double-bay beam is shown in Fig. 15. It
281 can be found that the beams keep straight at maximum MJD, which is similar to that of static tests.

282 Fig. 16 shows the horizontal displacement of the side columns of UPPC-DH. For exterior side
283 column, the maximum outward horizontal displacements of LHD1, LHD2, LHD3, LHD4, and LHD5
284 (refer to Fig. 16a) are -1.88 mm, -1.01 mm, -2.36 mm, -1.57 mm, and -0.23 mm, respectively. While
285 the maximum inward horizontal displacements are 3.97 mm, 4.62 mm, 5.18 mm, 4.27 mm and 3.12
286 mm, respectively. For interior side column, the maximum outward horizontal displacement of RHD1,

287 RHD2, RHD3, RHD4, and RHD5 (refer to Fig. 16b) are -0.49 mm, -0.81 mm, -1.15 mm, -0.73 mm,
288 and -0.46 mm, respectively, whereas the maximum inward horizontal displacement are 2.08 mm,
289 1.88 mm, 2.43 mm, 2.05 mm, and 1.01 mm, respectively. Therefore, similar to static tests, the
290 exterior side column experiences larger horizontal deformation than that of interior one. In general,
291 similar results are recorded in UPPC-DL.

292 4.3. Crack pattern and local damage

293 The crack pattern and local damage of UPPC-DL and UPPC-DH are illustrated in Figs. 17 and
294 18, respectively. The differences caused by different axial compression ratio are mainly reflected in
295 the crack pattern of the side columns. It could be found that the cracks observed in the side columns
296 of UPPC-DH are much fewer than that in UPPC-DL. Moreover, the cracks formed in the interior
297 column are milder than that in the exterior one for both specimens. Compared with their static
298 counterparts, UPPC-DL and UPPC-DH experiences similar damage at the similar displacement
299 stage (refer to Figs. 19 and 20). Therefore, it was confirmed that the dynamic effects will not change
300 the crack pattern and failure mode significantly. And the static push-down tests, which are most
301 commonly experimental method for progressive collapse studies, are able to equivalently
302 investigate the dynamic behavior of UPPC frames properly in terms of crack pattern and failure
303 mode.

304 4.4. Horizontal reaction force

305 Fig. 21 illustrates the total horizontal reaction force at each side of tested specimens. For
306 exterior side (without overhanging beam) of UPPC-DL, 1.0 s after suddenly removal of the column,
307 total horizontal reaction force reaches maximum compressive force of -71 kN a time of 1.388 s, but
308 then the compressive reaction force begins to decrease. At 1.71 s, the horizontal reaction force
309 changes from compressive to tensile. The maximum tensile force of 110 kN is measured at a time of
310 2.15 s. After vibration, the residual force of 89 kN is measured. For interior side (with overhanging
311 beam), the maximum horizontal compressive and tensile force are measured to be -84 kN and 185 kN
312 at times of 1.323 s and 1.97 s, respectively. Therefore, similar to static ones, the interior side achieves

313 larger compressive and tensile reaction force due to stronger horizontal restraints. For UPPC-DH, the
314 maximum horizontal compressive force at exterior side and interior side are -75 kN and -96 kN,
315 respectively, whereas the maximum horizontal tensile forces are 104 kN and 148 kN, respectively.
316 Therefore, both CAA and TCA are also measured in dynamic tests, which confirm that dynamic
317 effects will not change the load resisting mechanism of UPPC frames significantly. Moreover, it
318 should be noted that although sudden column removal tests are investigated in literature [36-38],
319 measuring dynamic horizontal reaction force after sudden column removal was very little.

320 Fig. 22 illustrates the contribution of each horizontal restraint to the total horizontal reaction
321 force. For exterior side of UPPC-DH, as shown in Fig. 22a, the bottom pin support contributes
322 majority of the compression force whereas the contribution from top roller is marginal. In tensile
323 phase, the contribution of tensile reaction force from top roller is similar to that from bottom pin
324 support. For the interior side, as shown in Fig. 22b, similar to the observation measured from the
325 exterior side, the bottom pin support contributes the majority of the compression force. However, in
326 tensile phase, the overhanging beam contributes the majority of the tensile force. In general, similar
327 trends are measured for UPPC-DL.

328 **5. Comparison of dynamic and quasi-static reaction force and prestressing force**

329 Fig. 23 compares the total horizontal reaction force from dynamic and quasi-static tests. For
330 UPPC-DL, the E-MHCF and I-MHCF are -71 kN and -84 kN, respectively. For UPPC-SL, the E-
331 MHCF and I-MHCF are -62 kN and -75 kN, respectively. In tension phase, when the UPPC-DL
332 (refer to Fig. 23a) reaches maximum displacement, the measured E-MHTF and I-MHTF are 110 kN
333 and 185 kN, respectively. For static specimen UPPC-SL, at the same displacement, the E-MHTF and
334 I-MHTF are 103 kN and 164 kN, respectively. As to UPPC-DH (refer to Fig. 23b), the E-MHCF, I-
335 MHCF, E-MHTF, and I-MHTF are -75 kN, -96 kN, 104 kN, and 148 kN, respectively. For static
336 specimen UPPC-SH, the E-MHCF, I-MHCF, E-MHTF, and I-MHTF are -67 kN, -84 kN, 92 kN, and
337 130 kN, respectively. Therefore, compared to static tests, the dynamic tests increase the horizontal
338 reaction force up by 15 % and 14 % for compressive and tensile phases, respectively. The DIF for
339 horizontal reaction force is up to 1.15.

340 Fig. 24 compares the total prestressing force from dynamic and quasi-static tests. The total
 341 initial prestressing force of UPPC-DL, UPPC-DH, UPPC-SL, and UPPC-SH are 242 kN, 241 kN,
 342 240 kN, and 238 kN, respectively. When the maximum MJD was reached, the prestressing forces of
 343 UPPC-DL and UPPC-DH are 322 kN and 318 kN, respectively. At the same MJD, the prestressing
 344 forces of UPPC-SL and UPPC-SH are 300 kN and 305 kN, respectively. Therefore, the increments of
 345 prestressing force in UPPC-SL and UPPC-SH are 25.0 % and 28.2 %, respectively, which are smaller
 346 than their dynamic counterparts (33.1 % and 32.0 % for UPPC-DL and UPPC-DH, respectively).

347 6. Analytical investigation

348 Due to complexity in construction, only two dynamic tests and two quasi-static tests were
 349 carried out in this study. To fully understand the dynamic response of UPPC frames and to predict
 350 their dynamic ultimate load capacity (DUL), a nonlinear single-degree-of-freedom (SDOF) model
 351 was developed. After validation, the SDOF model was also used to investigate the effects of applied
 352 load, no-zero initial condition, and damping ratio.

353 6.1. Development of the refined SDOF analytical model

354 Fig. 25 illustrates the refined SDOF model, which could consider the load resistance in
 355 declining phase well. The model consists of an equivalent mass (m_e) connected to a fixed boundary
 356 via a nonlinear spring ($k_e u(t)$) and viscous dashpot ($c_e \dot{u}(t)$). The SDOF model can be expressed as
 357 Eq. 2:

$$358 \quad m_e \ddot{u}(t) + c_e \dot{u}(t) + k_e u(t) = P(t) - R(t) \quad (2)$$

359 where m_e is the equivalent mass; c_e is a damping coefficient; k_e is an effective stiffness; $P(t)$ is the
 360 applied load, and $R(t)$ is the vertical resistance measured by the load cell (Item 14 in Fig. 2b), which
 361 was installed at SCRD. Note that, the m_e , c_e , and k_e of each specimen adopted in the SDOF model are
 362 correlated to their load resisting function, which were obtained from quasi-static tests.

363 6.2. Determination of m_e

364 As the shape function of the specimen is given, the equivalent mass can be determined by Eq. 3:

365
$$m_e = \int m(x)[\psi(x)]^2 dx + \sum_i m_i [\psi(x_i)]^2 \quad (3)$$

366 where $m(x)$ is the distributed mass function; $\psi(x)$ is the shape function; m_i is concentrated mass i
367 at location i , and $\psi(x_i)$ is shape function value at location i .

368 6.3. Determination of effective stiffness

369 As mentioned above, the effective stiffness is determined by the load resisting function measured
370 from quasi-static test. One of the most significant differences between the dynamic and quasi-static
371 test is strain rate effect (materials). According to the discussion in section “Comparison of dynamic
372 and quasi-static reaction”, the strain rate effect of material in this study is insignificant. Thus, it is
373 reasonable to predict the dynamic response of dynamic tested specimens based on the measured load
374 resisting function from static tests.

375 Another challenge is to determine the effective stiffness in post-yield stage. Reviewing previous
376 studies, it can be found that there are several prevalent approaches: 1. Sassani and Sagioglu [27]
377 proposed a bilinear load-displacement relationship and the declining phase were ignored; 2. Calvi et
378 al. [39] suggested to use secant stiffness at maximum displacement to consider post-yield strength of
379 the structure; 3. Yu and Guo [28] adopted tri-linear load function that is capable of considering the
380 resistance in declining phase. To obtain more accurate prediction, a more precise five-linear load
381 function was employed in this study to determine the effective stiffness.

382 The load resisting functions of UPPC-DL and UPPC-DH are given in Figs. 26a and b,
383 respectively. As shown in the figure, the load resisting functions consist of five linear segments (O-
384 A, A-B, B-C, C-D and D-E). As no obvious yield load was found, the stiffness in segment A-B was
385 set equal to the secant stiffness at the FPL. Beyond FPL, a load yield platform was formed. Thus, a
386 constant stiffness equal to secant stiffness at point B was used to represent segment A-B. Effective
387 stiffness of segment B-C was set equal to the slope of the load-displacement curve between point B
388 and C. Point C is the point at which the slope of the curve began to change significantly due to $P-\Delta$
389 effect. Stiffness at point D (SPL) and point E (drop by 20 % from the SPL) are set equal to their

390 secant stiffness while the points located in CD and DE can be determined by interpolation. The
391 effective stiffness of key points can be found in Table 5.

392 6.4. Effective damping coefficient c_e

393 As illustrated in Eq. 4, the effective damping coefficient is a function of damping ratio, effective
394 stiffness, and effective mass.

$$395 \quad c_e = 2\zeta\sqrt{k_e m_e} \quad (4)$$

396 The effective stiffness and effective mass are discussed above. Therefore, the main objective in
397 this section is to determine the damping ratio (ζ). As illustrated in Fig. 27, based on the logarithmic
398 decrement method, the damping ratios were determined as 12.5 % and 11.5 % for UPPC-DL and
399 UPPC-DH, respectively. The adopted effective damping coefficient for each segment can be easily
400 calculated by Eq. 4.

401 6.5. Applied load and vertical reaction measured in the SCRD

402 The steel weights would produce an equivalent concentrated load $P(t)$ at the column stub.
403 Meanwhile, the load cell (Item 14 in Fig. 2b) embedded in the SCRD would measure a vertical
404 reaction force $R(t)$ with same magnitude of $P(t)$. Fig. 25 illustrates the function of $P(t)$ and $R(t)$. $R(t)$
405 begins to reduce when the SCRD knocked down at a time of t_0 and reduce to zero when the SCRD
406 and the column stub separate completely at a corresponding time of $t_0 + \Delta t$. In general, for $R(t)$, a
407 nonlinear reduction function may be more realistic. However, as the column removal duration Δt is
408 quite small (0.008 s and 0.005 s for UPPC-DL and UPPC-DH, respectively), the assumption of linear
409 reduction of $R(t)$ has little effect on analytical results.

410 6.6. Validation of SDOF model

411 Fig. 28 compares the analytical displacement response to the measured ones. The predicted
412 maximum displacement of UPPC-DL and UPPC-DH are 344 mm and 318 mm at time of 2.09 s and
413 2.02 s, respectively, which were 107.6 % and 107.8 % of the measured one, respectively. Therefore,
414 the analytical curves agree with the measured ones well in term of maximum MJD as well as

415 corresponding time. However, the vibration after maximum MJD from the analytical curve is more
416 significant than that from tests. Moreover, the residual displacement from analytical model is less
417 than that from tests. This is because the effective stiffness of the model is determined based on the
418 measured load resisting function from monotonic tests. However, repeated vibration is observed in
419 the displacement response beyond the maximum MJD. Therefore, the proposed effective stiffness
420 method cannot reflect the stiffness of the dynamic specimen in the vibration stage beyond the
421 maximum MJD. It should be noted that, the maximum MJD is most important for evaluation of the
422 vulnerability of a frame to resist progressive collapse [26, 28] and thus the accuracy of validated
423 SDOF model was acceptable and the models were utilized for further parametric analysis.

424 6.7. Dynamic incremental analysis

425 *Effect of applied load*

426 In this section, the SDOF model was used to calculate the dynamic response of UPPC frame
427 under different load levels to predict the DUL of the specimens. As illustrated in Fig. 29, UPPC-DL
428 survived from an applied load (P in the legend) of 67 kN while failed to survived from 68 kN and
429 thus, the DUL of UPPC-DL was 67 kN. Similarly, the DUL of UPPC-DH was 61 kN.

430 Considering the dynamic increase factor (DIF) as a force-based factor [19], it can be determined
431 as follows:

$$432 \quad DIF = \frac{SUL}{DUL} \quad (5)$$

433 where SUL and DUL are the static and dynamic ultimate load, respectively.

434 Thus, the DIF of UPPC-DL and UPPC-DH are 1.34 and 1.28, respectively.

435 *Effect of non-zero initial condition*

436 If progressive collapse is triggered by extreme loading (e.g., gas explosions, impacts, vehicular
437 collisions or terrorist attacks), it always accompanied by a non-zero initial condition like non-zero
438 initial velocity and non-zero initial displacement. It is necessary to investigate the effect of non-zero
439 initial condition on the dynamic response.

440 Fig. 30 shows the dynamic response of UPPC-DH under different initial velocities. With initial
441 velocity of 0.5 m/s and -0.5 m/s, the maximum MJDs of UPPC-DH are determined as -342 mm and -
442 343 mm, respectively. Further increase the initial velocity to 0.75 m/s and -0.75 m/s, the maximum
443 MJDs are calculated as -371 mm and -376 mm, respectively. Therefore, both upward (positive value)
444 and downward (negative value) initial velocities will increase the maximum MJD, which can be
445 attributed to the additional kinematic involved.

446 Fig. 31 compares the MJD-time curves of UPPC-DH under different initial displacements. It can
447 be found that, when the initial upward (positive value) displacements of 50 mm and 100 mm are
448 given, the maximum MJDs are obtained as -340 mm and -362 mm, respectively. Thus, the initial
449 upward initial displacement will increase the maximum MJD. This is because the additional strain
450 energy due to initial upward displacement must be dissipated by the increased strain energy caused
451 by downward displacement. In contrast, the downward (negative value) initial displacement will
452 decrease the maximum MJD, as shown in the figure, with initial downward displacements of -50 mm
453 and -100 mm, the maximum MJDs reach -306 mm and -287 mm, respectively.

454 *Effect of damping ratio*

455 The effective of additional damper in resisting earthquake has been investigated extensively.
456 However, its merit in resisting progressive collapse attracted fewer attentions. Fig. 32 shows the
457 effect of damping ratio on the maximum MJD. As shown in the figure, under a given applied load of
458 40 kN, the maximum MJDs are -354 mm, -326 mm, -303 mm, and -285 mm, respectively, with
459 corresponding damping ratio of 5 %, 10 %, 15 %, and 20 %, respectively. The absolute value of the
460 maximum MJD is decreased by 19.5 % when the damping ratio increased from 5 % to 20 %.
461 Therefore, the benefits from large damping for mitigating progressive collapse are noticeable.
462 Additional dampers, which employed to resist earthquake was also effective for resisting progressive
463 collapse.

464 *Comparison of the results from SDOF model and energy-based method*

465 Energy-based method by Izzuddin et al. [25], is a simplified method to predict dynamic
466 resistance. Compared to SDOF model, the energy-based method may achieve conservative results

467 due to ignored damping effects. According to its assessment framework, the energy-based method is
468 mathematically expressed as:

$$469 \quad P_{CC}(u_d) = \frac{1}{u_d} \int_0^{u_d} P_{NS}(u) du \quad (6)$$

470 where $P_{CC}(u)$ and $P_{NS}(u)$ are the dynamic load resistance curve and static load resistance at the
471 displacement demand u , respectively.

472 As shown in Fig. 33, the DUL calculated by energy-based method are 55 kN and 53 kN,
473 respectively, for UPPC-SL and UPPC-SH. Based on SDOF model, the DUL of UPPC-SL and UPPC-
474 SH are 67 kN and 61 kN, respectively. Therefore, for UPPC-SL and UPPC-SH, the DULs obtained
475 from SDOF model are higher than that from energy-based method by 21.8 % and 15.1 %,
476 respectively.

477

478 **7. Conclusions**

479 In this paper, a comparative study on experimental tests of four UPPC frames under quasi-static
480 and dynamic loading regimes are performed to investigate the progressive collapse capacity of UPPC
481 frames subjected to a penultimate column removal scenario. Moreover, a refined SDOF model was
482 developed in this research and validated. Then, it was used to conduct dynamic incremental analysis.
483 Based on experimental results and discussion, the following conclusions can be drawn:

- 484 1. The failure modes of UPPC frames are quite similar in both quasi-static and dynamic test.
485 However, they are quite different to that of RC frames mainly due to discontinuous beam
486 reinforcements. Therefore, no plastic hinges were formed at the beam ends whereas wide
487 openings were concentrated at the beam-column interfaces. The damage of beam was
488 concentrated at compressive toes but no cracks occurred along the beam. When a penultimate
489 column was assumed to be lost, the failure of UPPC frame was controlled by large eccentric
490 compressive failure in the exterior side column.
- 491 2. For dynamic tests, specimens with higher axial compression ratio experienced much milder
492 damage. For quasi-static tests, higher axial compression ratio could increase the first peak load

- 493 slightly. However, it resulted in greater P- Δ effect at large deformation stage, which may result
494 in pre-mature failure with less deformation capacity and second peak load.
- 495 3. The reliability of the column removal apparatus was proved to be satisfactory. The column
496 removal durations were 0.008 s and 0.005 s for UPPC-DL and UPPC-DH, respectively, which
497 well satisfied the requirements of DoD [13] that the column removal duration should be less than
498 1/10 of the natural period of the vibration.
- 499 4. Large damping ratio was demonstrated to have noticeable benefits in resisting progressive
500 collapse. Non-zero initial velocity and initial upward displacement would increase the maximum
501 dynamic displacement whereas initial downward displacement would decrease the maximum
502 dynamic displacement. The dynamic increase factor of UPPC-DL and UPPC-DH were
503 determined to be 1.34 and 1.28, respectively. However, for horizontal reaction force, the
504 maximum dynamic increase factor was 1.15. Therefore, the dynamic increase factor was
505 different even in a single dynamic test when different response was focused on.
- 506 5. Compared to the SDOF model, it was validated that the energy-based assessment framework
507 proposed by Izzuddin et al. [24] predicted a more conservative dynamic progressive collapse
508 resistance of UPPC frames due to ignored damping effects.

509 **Acknowledgements**

510 The authors gratefully acknowledge the financial support provided by the Natural Science
511 Foundation of China (Nos. 51778153, 51568004, 51478118). Any opinions, findings and conclusions
512 expressed in this paper do not necessary reflect the view of Natural Science Foundation of China.

513

514 **References**

- 515 [1] Priestley MJN. Overview of the PRESSS research program. PCI J 1991; 36(4):50-57.
- 516 [2] Stone WC, Cheok GS, Stanton JF. Performance of hybrid moment-resisting precast beam-
517 column concrete connection subjected to cyclic loading. ACI Struct J 1995; 92(2):229-49.
- 518 [3] Stanton J, Stone WC, Cheok GS. A hybrid reinforced precast frame for seismic regions. PCI J
519 1997; 42(2):20-32.

- 520 [4] Morgen BG, Kurama YC. A friction damper for post-tensioned precast concrete moment frames.
521 PCI J 2004; 49(4):112-32.
- 522 [5] Li L, Mander JB, Dhakal RP. Bi-directional cyclic loading experiment on a 3-D beam-column
523 joint designed for damage avoidance, J Struct Eng 2008; 134(11):1733–42.
- 524 [6] Solberg KM, Dhakal RP, Bradley BA, Mander JB, Li L. Seismic performance of damage-
525 protected beam–column joints. ACI Struct J 2008; 105(2):205–14.
- 526 [7] Bradley BA, Dhakal RP, Mander JB, Li L. Experimental multi-levels seismic performance
527 assessment of 3D RC frame designed for damage avoidance. Earthquake Eng and Struct Dyn
528 2008; 37(1):1-20.
- 529 [8] Song LL, Guo T, Chen C. Experimental and numerical study of a self-centering prestressed
530 concrete moment resisting frame connection with bolted web friction devices. Earthquake Eng
531 Struct Dyn 2014; 43(4):529–45.
- 532 [9] Song LL, Guo T, Gu Y, Cao ZL. Experimental study of a self-centering prestressed concrete
533 frame subassembly. Eng Struct 2015; 88:176–88.
- 534 [10] Song LL, Guo T, Gu Y, Cao ZL. Seismic response of self-centering prestressed concrete moment
535 resisting frames with web friction devices. Soil Dyn Earthq Eng 2015; 71:151-62.
- 536 [11] Lu XZ, Zhang L, Lin KQ, Li Y. Improvement to composite frame systems for seismic and
537 progressive collapse resistance. Eng Struct 2019; 186:227-42.
- 538 [12] Qian K, Liang SL, Fu F, Fang Q. Progressive collapse resistance of precast concrete beam-
539 column sub-assemblages with high-performance dry connections. Eng Struct 2019; 198:109552.
- 540 [13] Department of Defense (DoD). Design of building to resist progressive collapse. Unified facility
541 criteria, UFC 4-023-03, Washington, DC; 2010.
- 542 [14] Sadek F, Main J, Lew H, Bao Y. Testing and analysis of steel and concrete beam-column
543 assemblies under a column removal scenario. J Struct Eng 2011; 137(9):881–92.
- 544 [15] Qian K, Li B. Performance of three-dimensional reinforced concrete beam-column substructures
545 under loss of a corner column scenario. J Struct Eng 2013; 139(4):584-94.
- 546 [16] Qian K, Li B. Slab effects on response of reinforced concrete substructures after loss of corner
547 column. ACI Struct J 2012; 109:845-55.
- 548 [17] Yu J, Tan K H. Structural behavior of reinforced concrete beam-column sub-assemblages under
549 a middle column removal scenario. J Struct Eng 2013; 139(2):233-50.
- 550 [18] Valipour H, Vessali N, Foster SJ, Samali B. Influence of concrete compressive strength on the
551 arching behaviour of reinforced concrete beam assemblages. Int J Adv Struct Eng 2015; 18(8):
552 1199-214.
- 553 [19] Quiel SE, Naito CJ, Fallon CT. A non-emulative moment connection for progressive collapse
554 resistance in precast concrete building frames. Engineering Structures 2019; 179:174-188.

- 555 [20] Qian K, Li B. Dynamic performance of RC beam-column substructures under the scenario of the
556 loss of a corner column—Experimental results. *Eng Struct* 2012; 42:154-67.
- 557 [21] Qian K, Li B. Quantification of slab influences on the dynamic performance of RC frames
558 against progressive collapse. *J Perform Constr Facil* 2015; 29(1):04014029.
- 559 [22] Yu J, Rinder T, Stolz A, Tan K H, Riedel W. Dynamic progressive collapse of an RC
560 assemblage induced by contact detonation. *J Struct Eng* 2014; 140(6):04014014.
- 561 [23] Russell JM, Owen JS, Hajirasouliha I. Experimental investigation on the dynamic response of
562 RC flat slabs after a sudden column loss. *Eng Struct* 2015; 99:28-41.
- 563 [24] Qian K, Weng YH, Li B. Improving behavior of reinforced concrete frames to resist progressive
564 collapse through steel bracings. *J Struct Eng* 2019; 145(2):04018248.
- 565 [25] Izzuddin B, Vlassis A, Elghazouli A, Nethercot D. Progressive collapse of multistorey buildings
566 due to sudden column loss-Part I: Simplified assessment framework. *Eng Struct* 2008; 30:1308–
567 18.
- 568 [26] Tsai MH. An analytical methodology for the dynamic amplification factor in progressive
569 collapse evaluation of building structures. *Mech Res Commun* 2010; 37(1):61–66.
- 570 [27] Sasani M, Sagioglu S. Progressive collapse of reinforced concrete structures: A multihazard
571 perspective. *ACI Struct J* 2008; 105(1):96–103.
- 572 [28] Yu J, Guo YQ. Nonlinear SDOF model for dynamic response of structures under progressive
573 collapse. *J Eng Mech* 2016; 142(3):04015103.
- 574 [29] ACI Committee 318, Building Code Requirements for Structural Concrete (ACI 318-14) and
575 Commentary (318R-14). American Concrete Institute, Farmington Hills, MI, 433 pp; 2014.
- 576 [30] Su YP, Tian Y, Song XS. Progressive collapse resistance of axially-restrained frame beams. *ACI*
577 *Struct J* 2009; 106(5):600–7.
- 578 [31] Yu J, Tan KH. Special detailing techniques to improve structural resistance against progressive
579 collapse. *J Struct Eng* 2014; 140(3):04013077.
- 580 [32] Kang SB, Tan KH. Behaviour of precast concrete beam-column sub-assemblages subject to
581 column removal. *Eng Struct* 2015; 93:85–96.
- 582 [33] Nimse RB, Joshi DD, Oatel PV. Behavior of wet precast beam column connections under
583 progressive collapse scenario: an experimental study. *Int J Adv Struct Eng* 2014; 6(4):149–59.
- 584 [34] Al-Salloum YA, Alrubaidi MA, Elsanadedy HM, Almusallam TH. Strengthening of precast RC
585 beam-column connections for progressive collapse mitigation using bolted steel plates.
586 *Engineering Structures* 2018; 161:146-160.
- 587 [35] Zhou Y, Chen TP, Pei YL, Hwang HJ, Hu X, Yi WJ. Static load test on progressive collapse
588 resistance of fully assembled precast concrete frame structure. *Engineering Structures* 2019;
589 200:109719.

- 590 [36] Sasani M. Response of a reinforced concrete infilled-frame structure to removal of two adjacent
591 columns. *Eng Struct* 2008; 30(9):2478–91
- 592 [37] Sasani M, Sagioglu S. Gravity load redistribution and progressive collapse resistance of 20-
593 story reinforced concrete structure following loss of interior column. *ACI Struct J* 2010;
594 107(6):636–44.
- 595 [38] Sasani M, Kazemi A, Sagioglu S, Forest S. Progressive collapse resistance of an actual 11-story
596 structure subjected to severe initial damage. *J Struct Eng* 2011; 137(9):893–902.
- 597 [39] Calvi G M, Priestley M J N, Kowalsky MJ. *Displacement-based seismic design of structures*,
598 IUSS Press, Pavia, Italy, 2008.

599

600

601

602

603

604

605

606

607

608

609

610

611

612

613

614

615

616

617

618

619

620

621

622

623

624

625

626

627

Table 1-Specimen information

Specimen ID	Element Size			span/depth ratio	Axial compression ratio	Effective prestress	Loading approach
	Span (mm)	Beam (mm×mm)	Column (mm×mm)				
UPPC-SL	2750	150×250	250×250	11	0.2	0.65 f_{pu}	Static
UPPC-SH	2750	150×250	250×250	11	0.4	0.65 f_{pu}	Static
UPPC-DL	2750	150×250	250×250	11	0.2	0.65 f_{pu}	Dynamic
UPPC-DH	2750	150×250	250×250	11	0.4	0.65 f_{pu}	Dynamic

628

Note: f_{pu} is the nominal ultimate strength of the unbounded post-tensioned strands (1860 MPa).

629

630

631

Table 2-Material properties

Item	Nominal diameter (mm)	Yield strength (MPa)	Ultimate strength (MPa)	Elastic modulus (MPa)	Elongation (%)
Stirrups R6	6	368	485	162,000	20.1
Beam reinforcements T12	12	462	596	171,000	14.7
Column reinforcements T16	16	466	604	182,000	17.0
Unbonded strands	12.7	1,649	1,970	213,000	6.3

632

633

634

Table 3- Definition of abbreviations

MJD	Middle Joint Displacement
MMJD	Maximum Middle Joint Displacement
FPL	First Peak Load
SPL	Second Peak Load
E-MHCF	Maximum Horizontal Compressive Force on Exterior Side
I-MHCF	Maximum Horizontal Compressive Force on Interior Side
E-MHTF	Maximum Horizontal Tensile Force on Exterior Side
I-MHTF	Maximum Horizontal Tensile Force on Interior Side
SUL	Static Ultimate Load
DUL	Dynamic Ultimate Load

635

636

637

Table 4-Test results

Specimen ID	FPL (kN)	SPL (kN)	E-MHCF (kN)	I-MHCF (kN)	E-MHTF (kN)	I-MHTF (kN)	MMJD (mm)
UPPC-SL	39	90	-62	-75	135	259	N/A
UPPC-SH	41	78	-67	-84	156	253	N/A
UPPC-DL	N/A	N/A	-71	-84	110	185	320
UPPC-DH	N/A	N/A	-75	-96	104	148	295

638

Note: FPL and SPL represent first peak load and second peak load, respectively; I-MHCF/I-MHTF and E-MHCF/E-MHTF represent maximum horizontal compressive /tensile force on interior and exterior side, respectively; MMJD represents maximum middle joint displacement

639

640

641

Table 5-Parameters in SDOF model and analytical results

Specimen ID	m_e (kg)	k_A (kN/m)	k_B (kN/m)	k_C (kN/m)	k_D (kN/m)	k_E (kN/m)	MMJD (mm)	DUL	$\frac{SUL}{DUL}$
UPPC-DL	18006	1258	150	190	152	106	344	67	1.34
UPPC-DH	18006	1367	165	222	169	107	318	61	1.28

642

Note: MMJD represents maximum middle joint displacement; DUL and SUL represent dynamic ultimate load and static ultimate load, respectively.

643

644 **List of Figures**

645 **Fig. 1** Details of test specimen: (a) global details; (b) joint details; (c) section details

646 **Fig. 2** Test setup: (a) quasi-static test-photo; (b) dynamic test-photo; (c) dynamic test-drawing

647 **Fig. 3** Vertical load-displacement curves

648 **Fig. 4** Failure mode of UPPC-SL

649 **Fig. 5** Failure mode of UPPC-SH

650 **Fig. 6** Deflection of the double-bay beam of UPPC-SL

651 **Fig. 7** Horizontal drift in side columns of UPPC-HL: (a) exterior side column; (b) interior side
652 column

653 **Fig. 8** Horizontal reaction of UPPC-SH: (a) exterior side; (b) interior side

654

655 **Fig. 9** Variation of bending moment in the exterior side column

656 **Fig. 10** Determination of the failure mode of the exterior side column

657 **Fig. 11** Load resisting mechanism in UPPC frame: (a) MJD smaller than one beam depth; (b) MJD
658 beyond one beam depth

659 **Fig. 12** Load resistance decomposition of test specimens: (a) UPPC-SL; (b) UPPC-SH

660 **Fig. 13** Column removal duration

661 **Fig. 14** Deflection of the double-bay beam: (a) UPPC-DL; (b) UPPC-DH

662 **Fig. 15** Deformation shapes of the double-bay beam

663 **Fig. 16** Horizontal displacement in side column of UPPC-DH: (a) exterior side column; (b) interior
664 side column

665 **Fig. 17** Crack pattern and local damage of UPPC-DL

666 **Fig. 18** Crack pattern and local damage of UPPC-DH

667 **Fig. 19** Crack pattern and local damage of UPPC-SL at MJD of 320 mm

668 **Fig. 20** Crack pattern and local damage of UPPC-SH at MJD of 295 mm

669 **Fig. 21** Total horizontal reaction-time curves

670 **Fig. 22** Horizontal reaction of UPPC-DH: (a) exterior side; (b) interior side

671 **Fig. 23** Comparison of the total horizontal reaction: (a) UPPC-SL vs. UPPC-DL; (b) UPPC-SH vs.
672 UPPC-DH
673 **Fig. 24** Variation of prestressing forces in strands
674 **Fig. 25** Simplified SDOF model
675 **Fig. 26** Load resisting function: (a) UPPC-SL; (b) UPPC-SH
676 **Fig. 27** Determination of damping ratio: (a) UPPC-DL; (b) UPPC-DH
677 **Fig. 28** Comparison of the theoretical MJD to the measured one: (a) UPPC-DL; (b) UPPC-DH
678 **Fig. 29** Determination of dynamic ultimate load
679 **Fig. 30** Effect of initial velocity
680 **Fig. 31** Effect of initial displacement
681 **Fig. 32** Effect of damping ratio
682 **Fig. 33** Dynamic resistance based on energy method
683
684
685
686
687
688
689
690
691
692
693
694
695
696
697
698
699
700
701

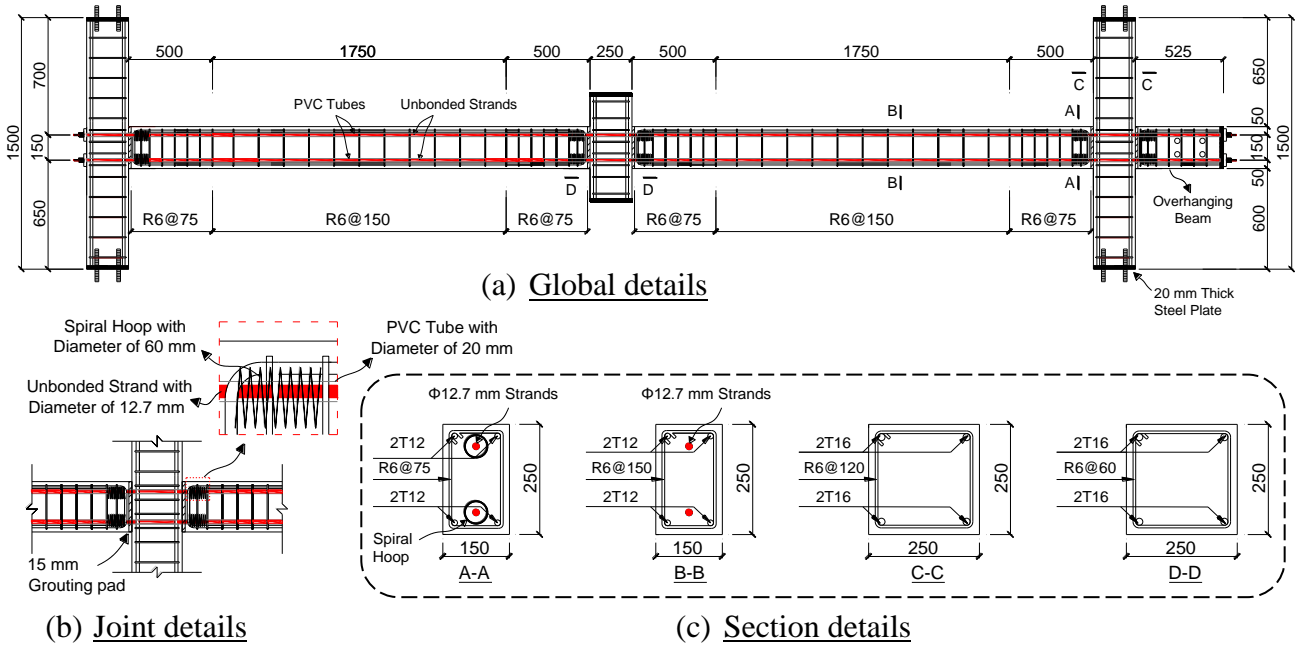
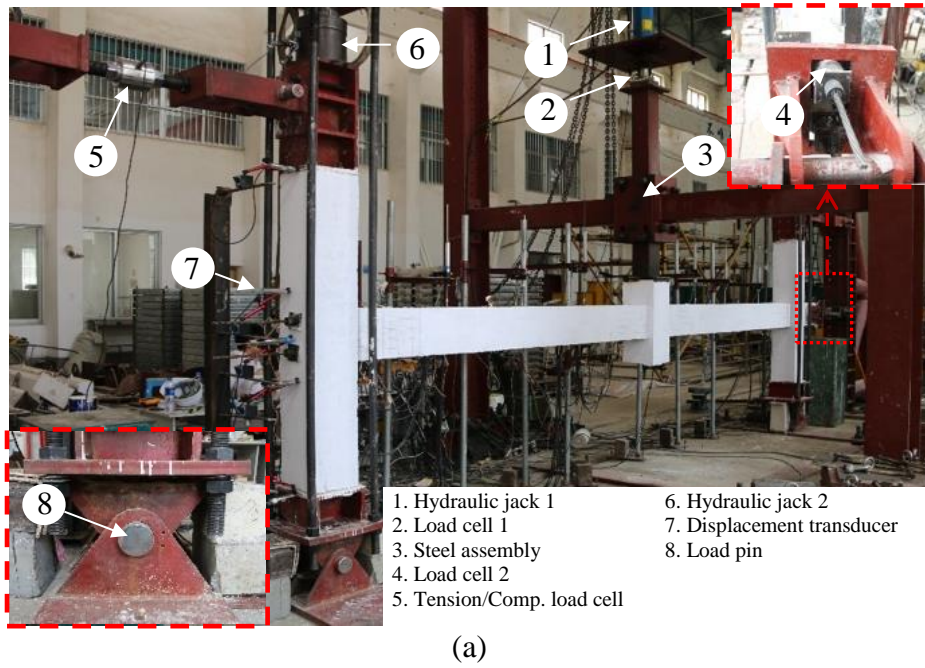


Fig. 1 Details of test specimen: (a) global details; (b) joint details; (c) section details



718
719

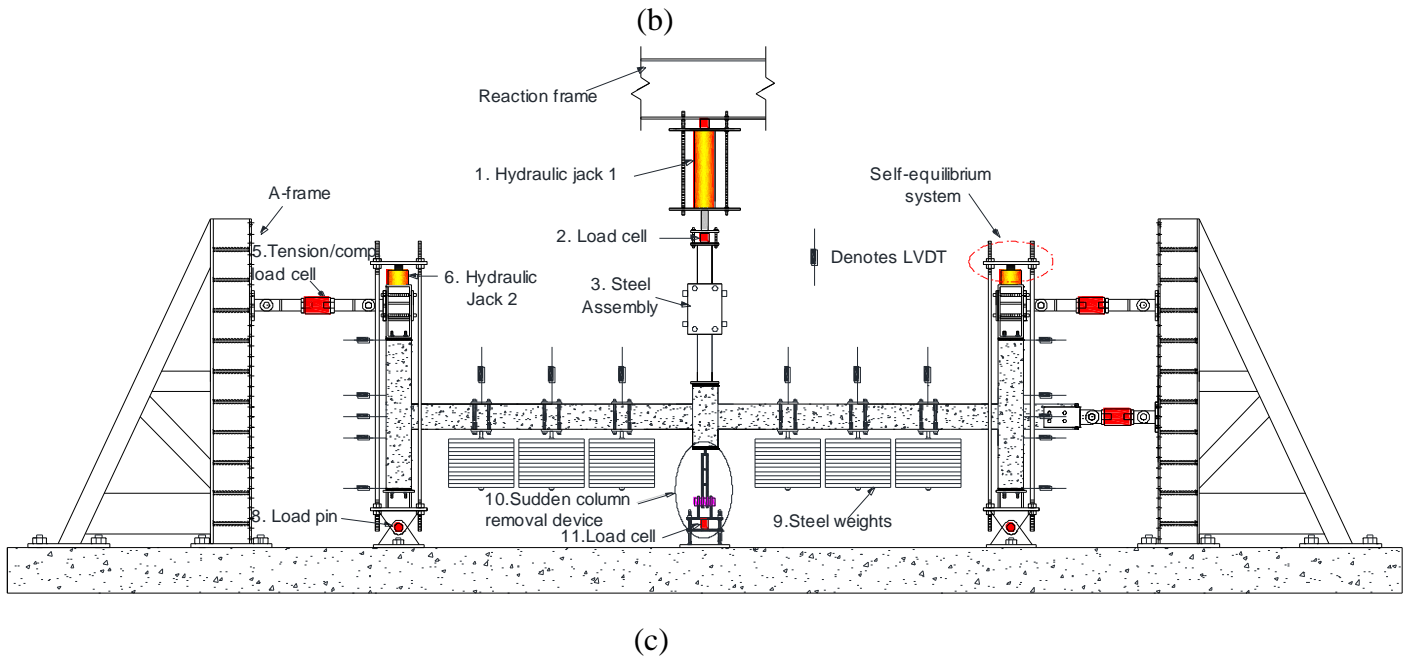
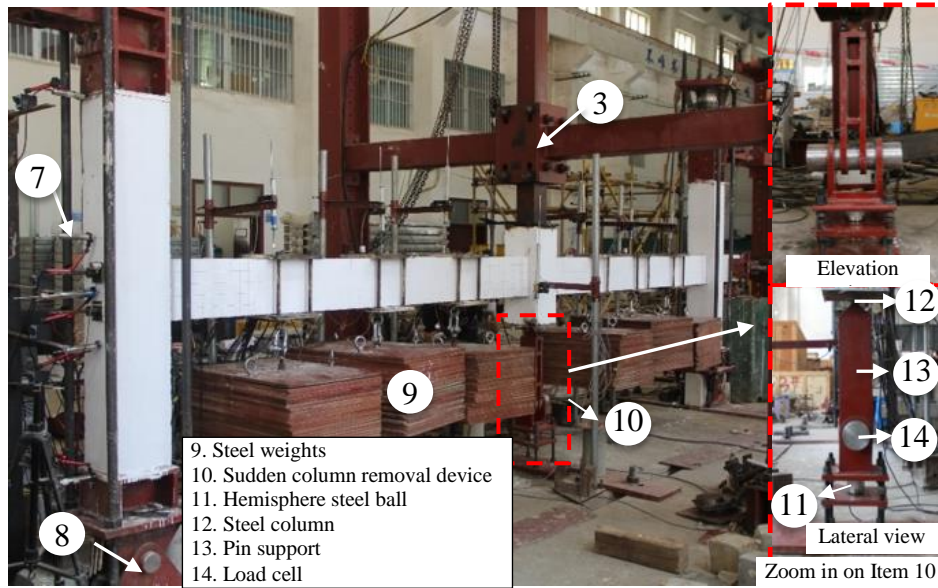


Fig. 2 Test setup: (a) quasi-static test-photo; (b) dynamic test-photo; (c) dynamic test-drawing

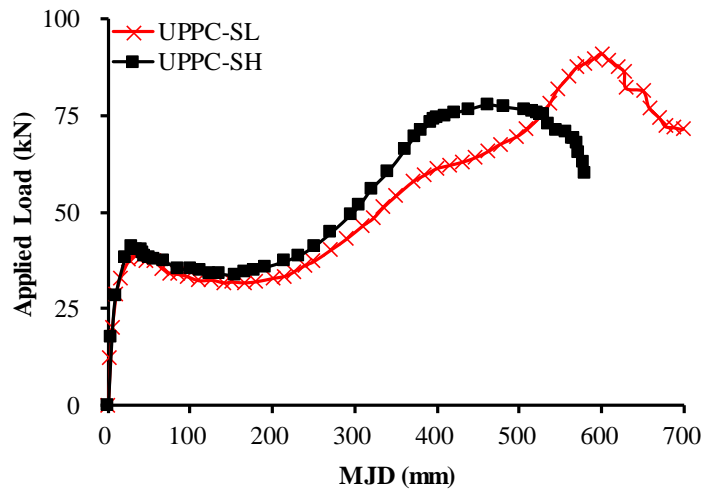


Fig. 3 Vertical load-displacement curves

729
730

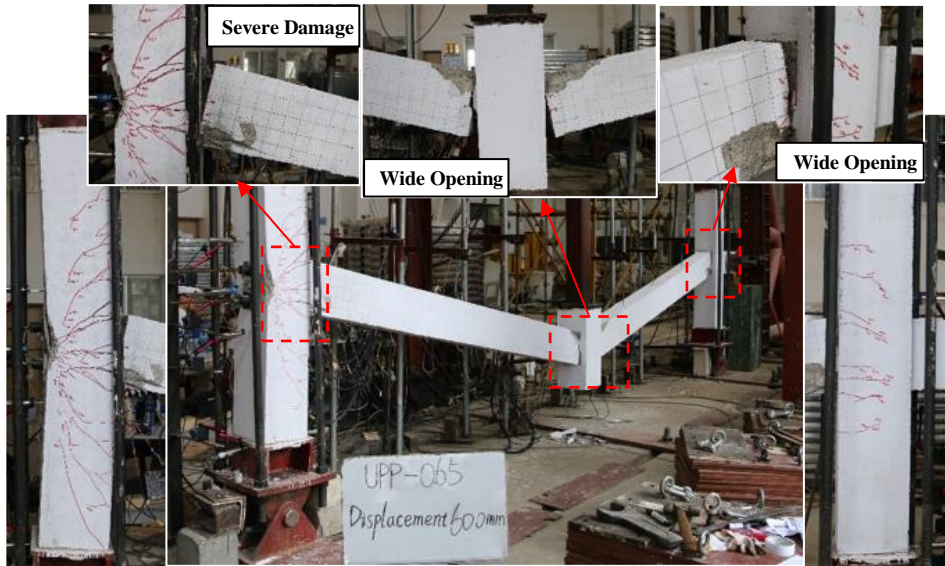


Fig. 4 Failure mode of UPPC-SL

731
732
733
734

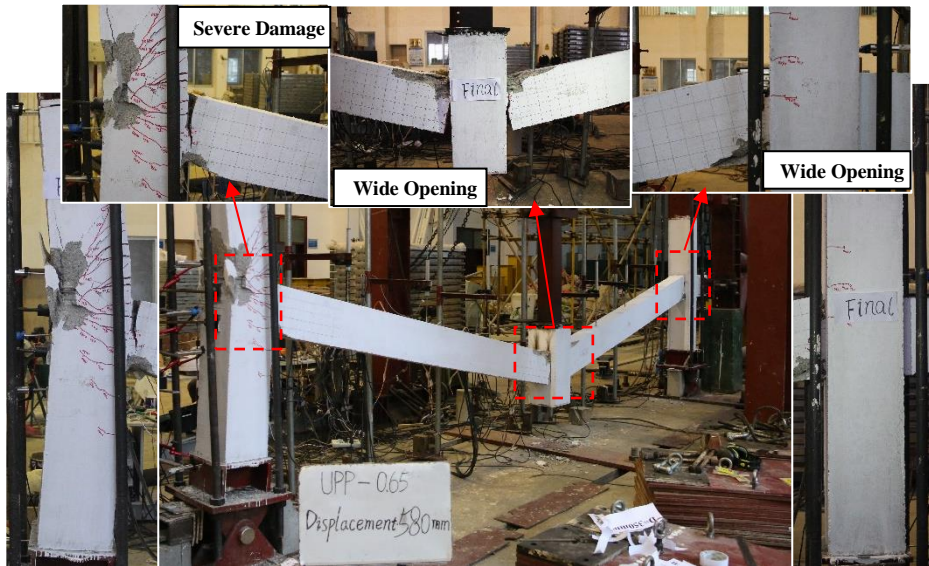


Fig. 5 Failure mode of UPPC-SH

735
736
737

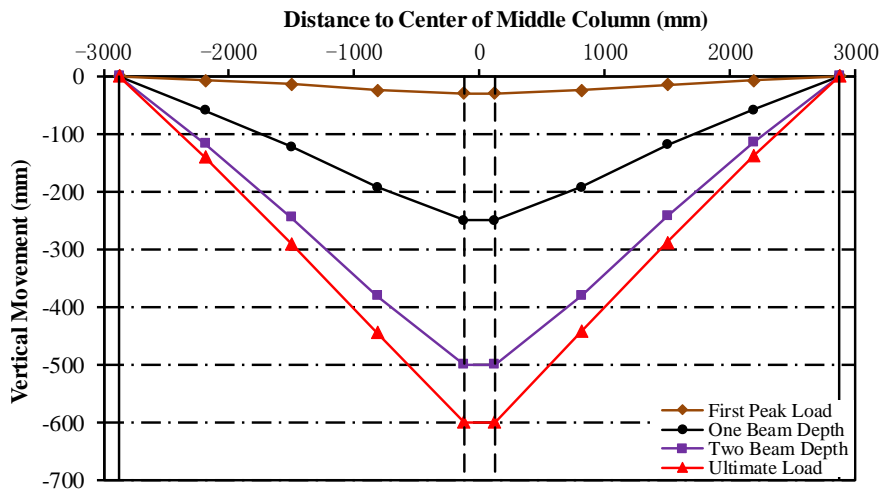
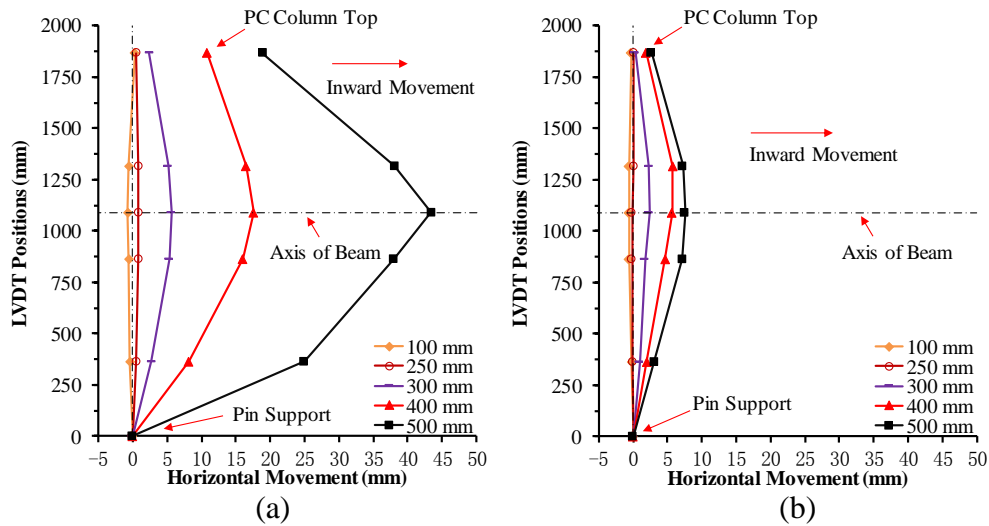


Fig. 6 Deflection of the double-bay beam of UPPC-SL

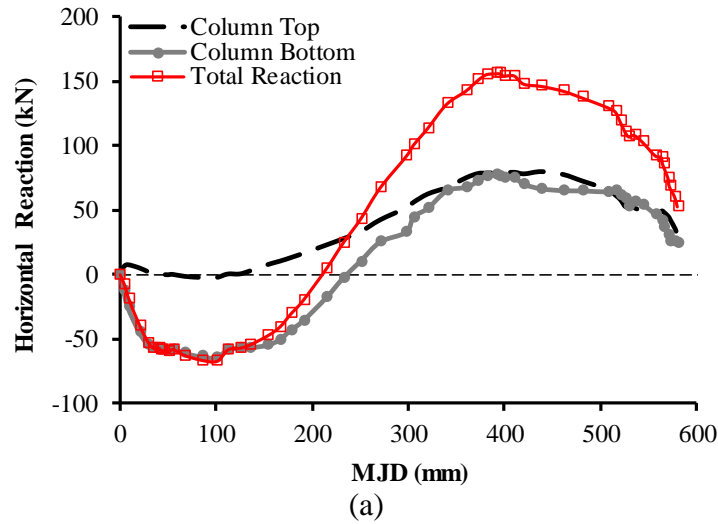
738
739
740

741
742

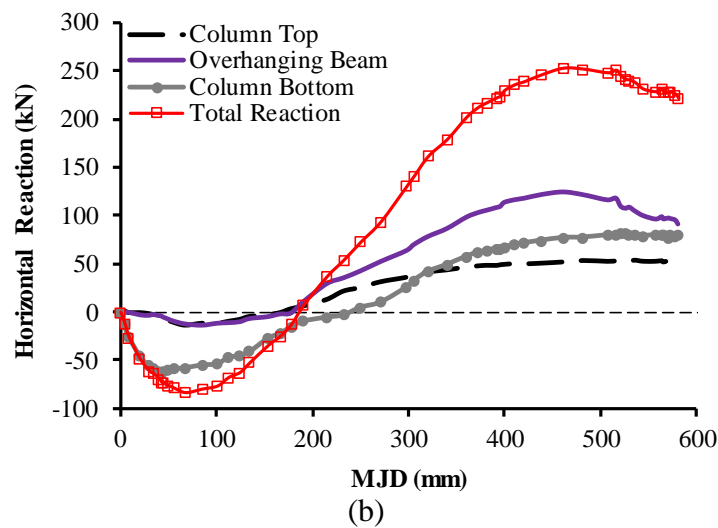


743
744
745
746
747
748

Fig. 7 Horizontal drift in side columns of UPPC-HL: (a) exterior side column; (b) interior side column



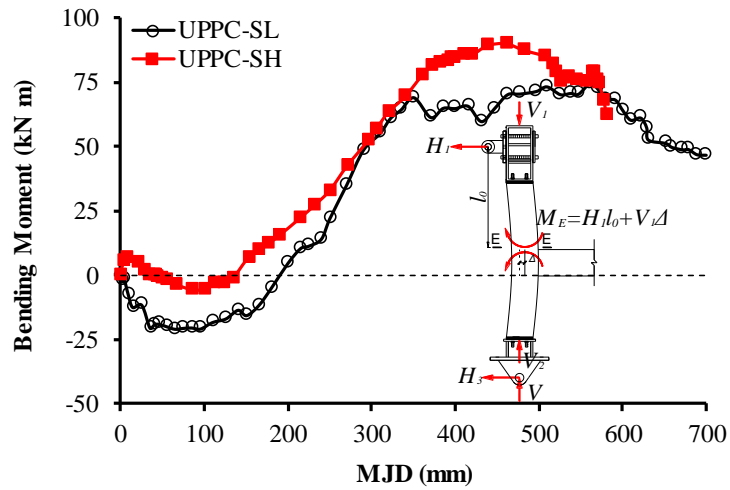
749
750
751
752



753
754
755
756
757

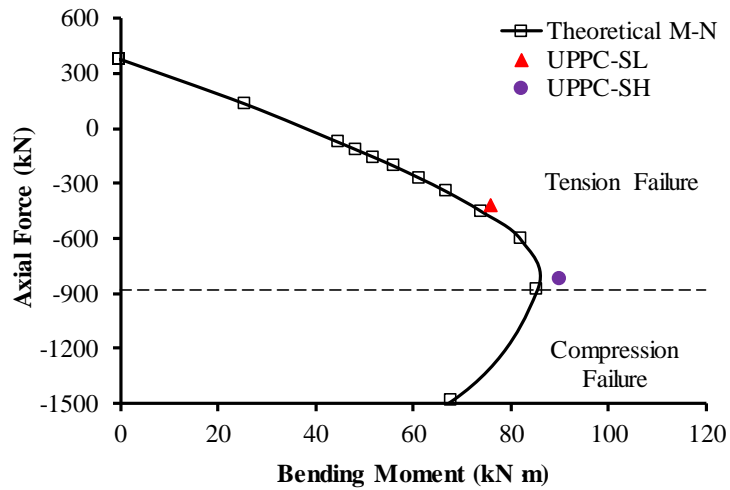
Fig. 8 Horizontal reaction of UPPC-SH: (a) exterior side; (b) interior side

758
759



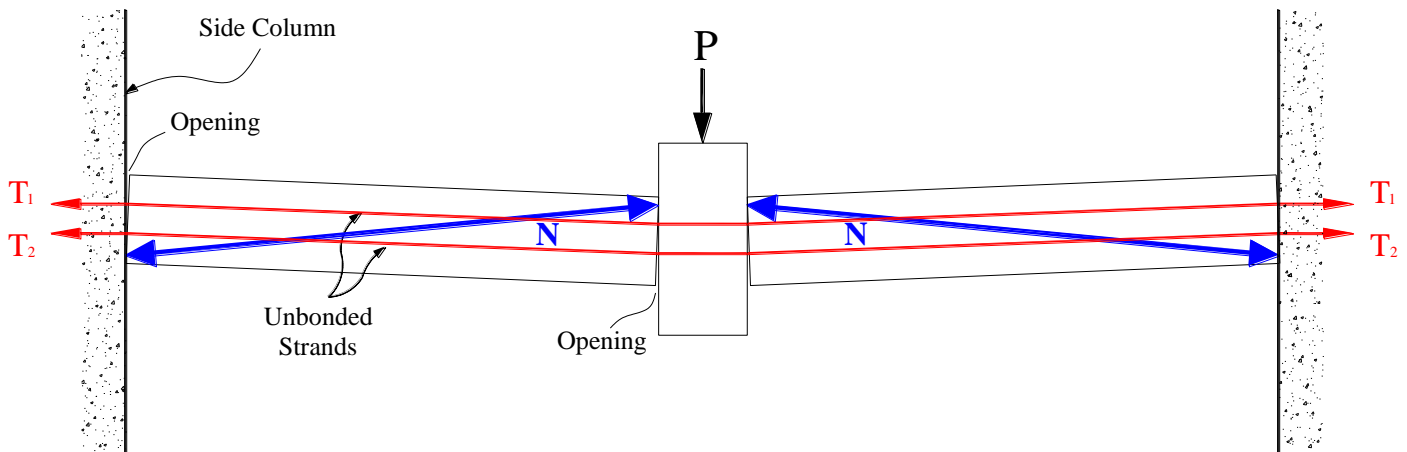
760
761 **Fig. 9** Variation of bending moment in the exterior side column

762
763
764

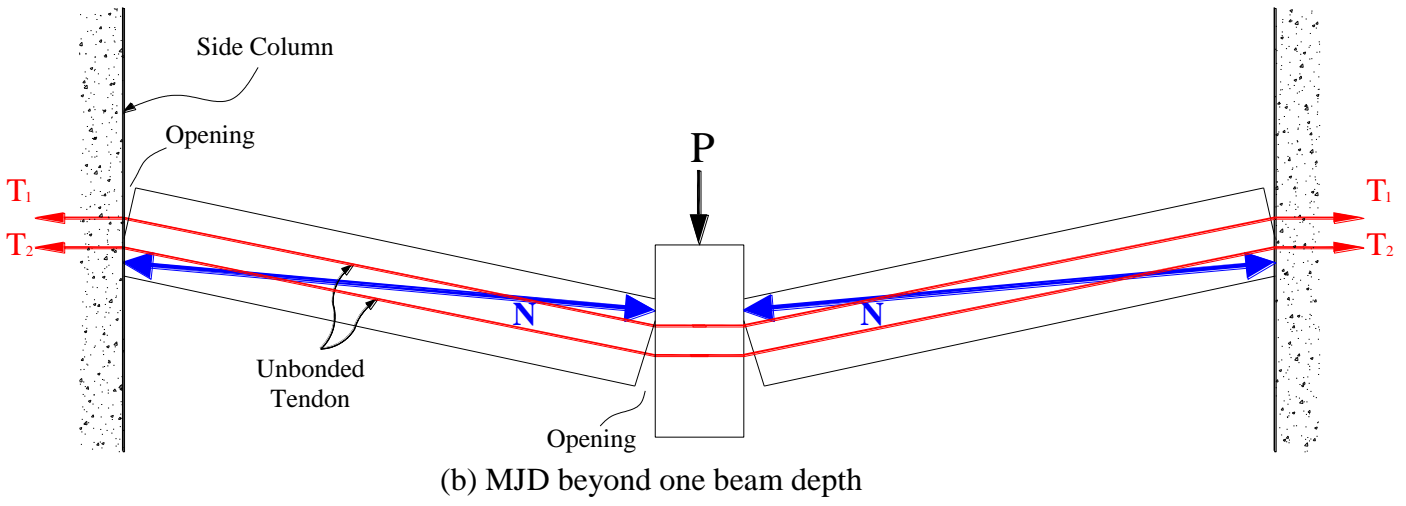


765
766 **Fig. 10** Determination of the failure mode of the exterior side column

767

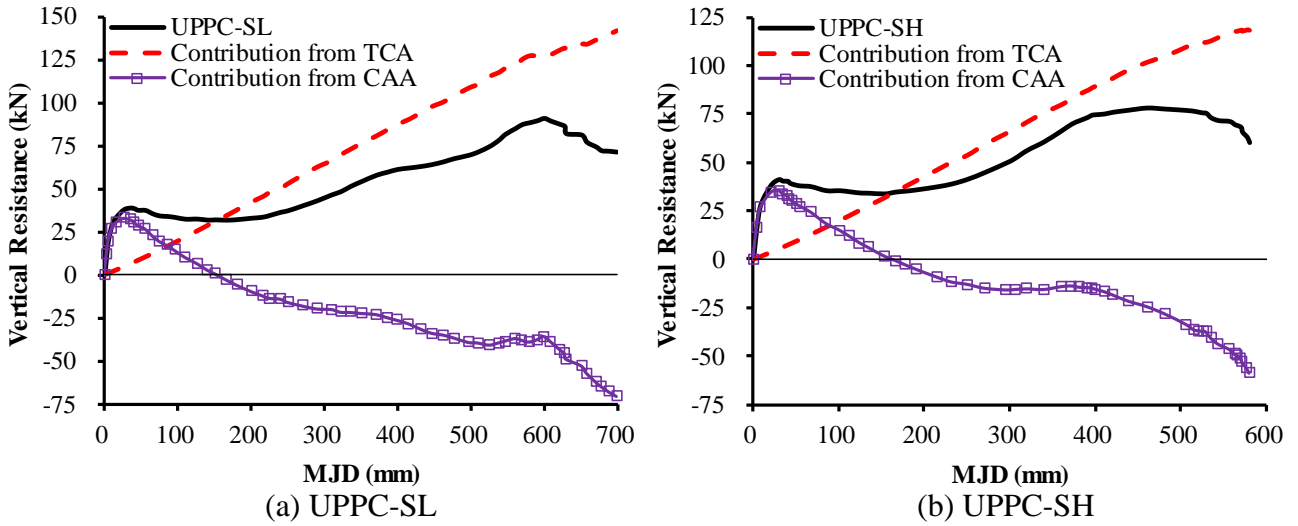


768
769 (a) MJD smaller than one beam depth



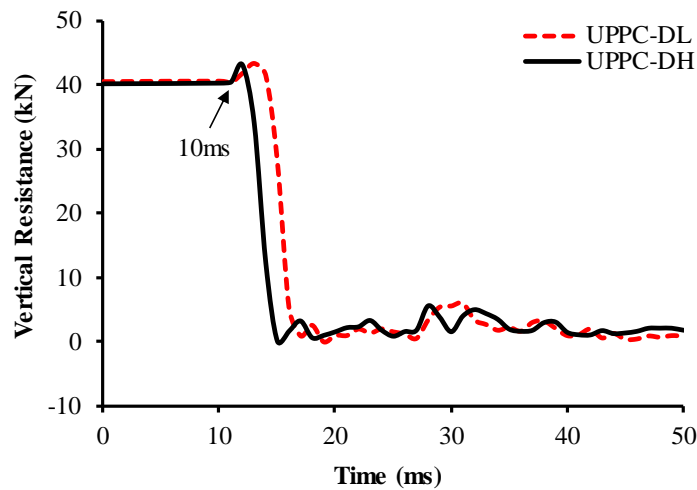
770
771
772
773
774
775
776
777
778

Fig. 11 Load resisting mechanism in UPPC frame: (a) MJD smaller than one beam depth; (b) MJD beyond one beam depth



779
780
781
782
783

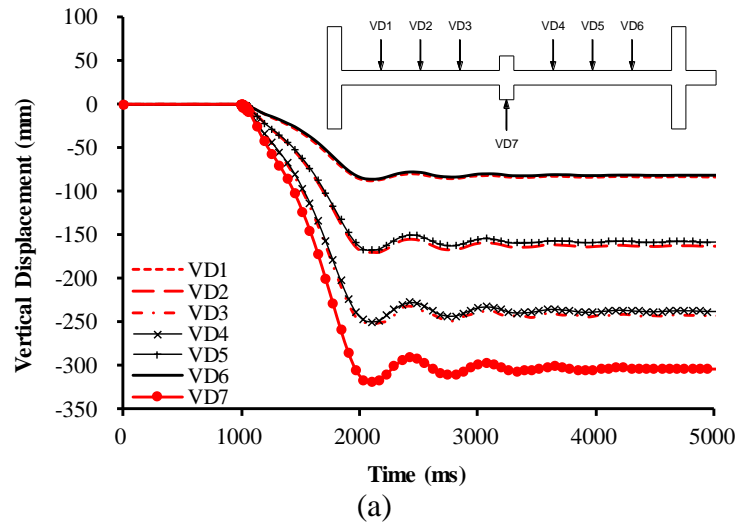
Fig. 12 Load resistance decomposition of test specimens: (a) UPPC-SL; (b) UPPC-SH



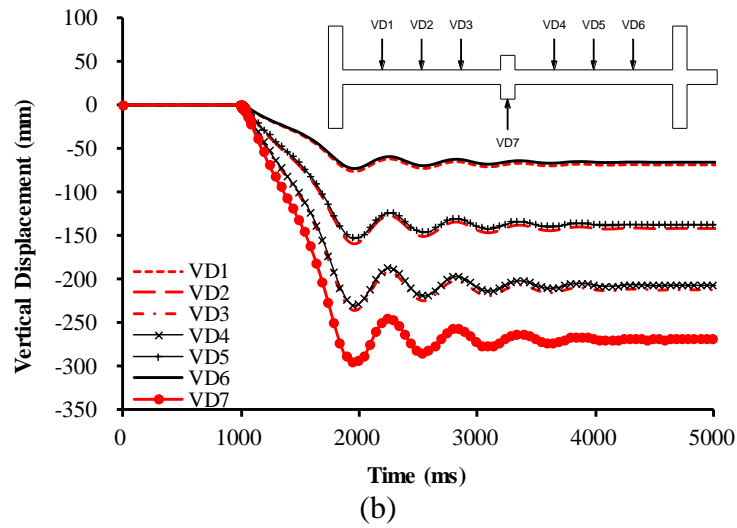
784
785
786
787

Fig. 13 Column removal duration

788
789

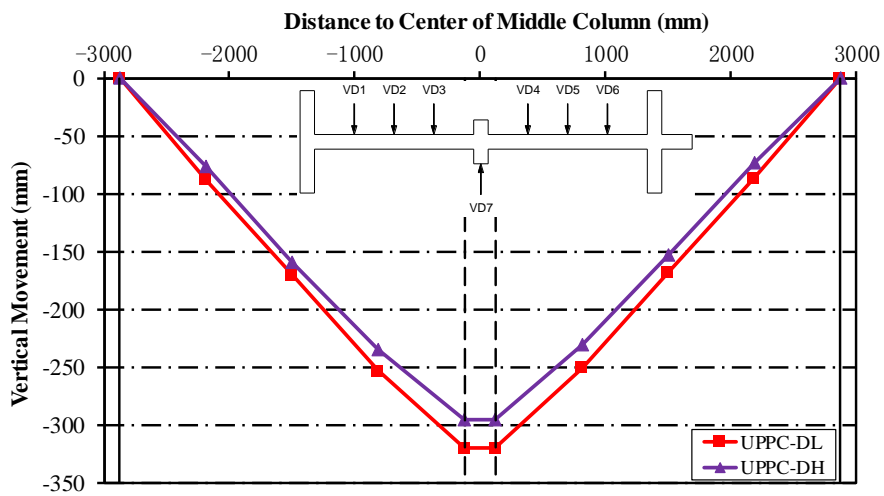


790
791
792
793



794
795
796
797
798
799

Fig. 14 Deflection of the double-bay beam: (a) UPPC-DL; (b) UPPC-DH



800
801
802
803
804

Fig. 15 Deformation shapes of the double-bay beam

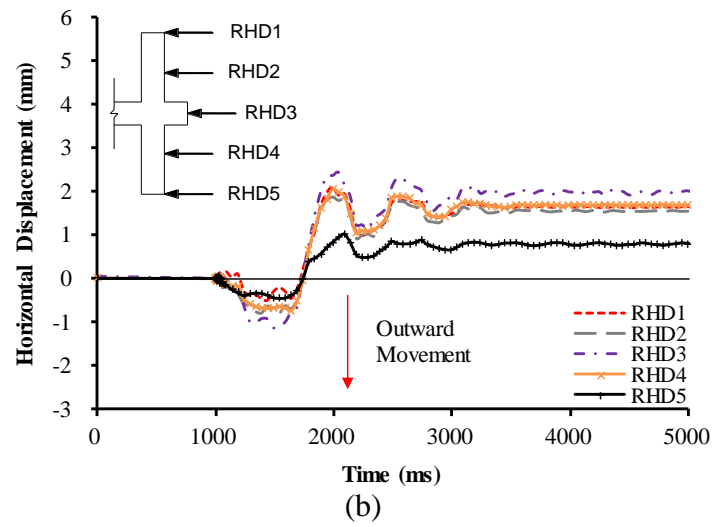
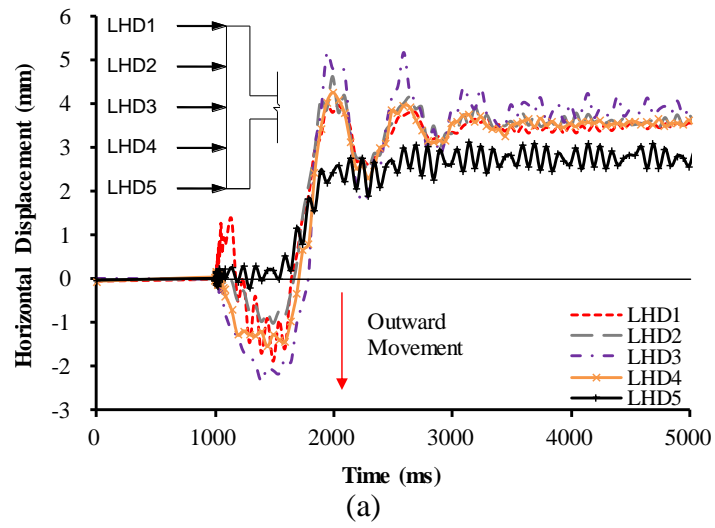


Fig. 16 Horizontal displacement in side column of UPPC-DH: (a) exterior side column; (b) interior side column

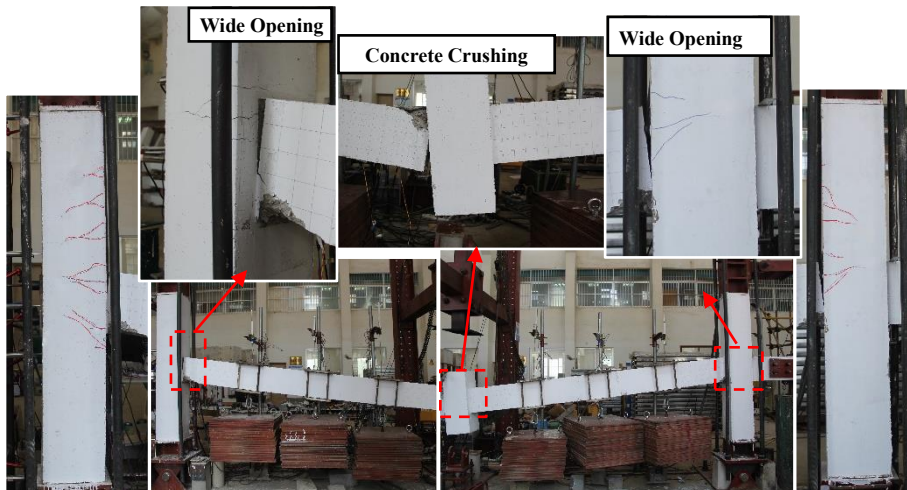


Fig. 17 Crack pattern and local damage of UPPC-DL

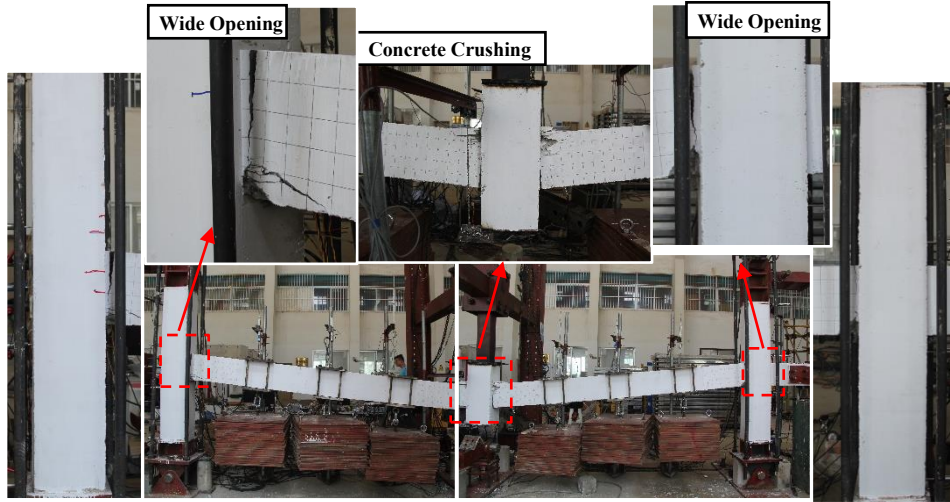


Fig. 18 Crack pattern and local damage of UPCC-DH

823
824
825
826
827

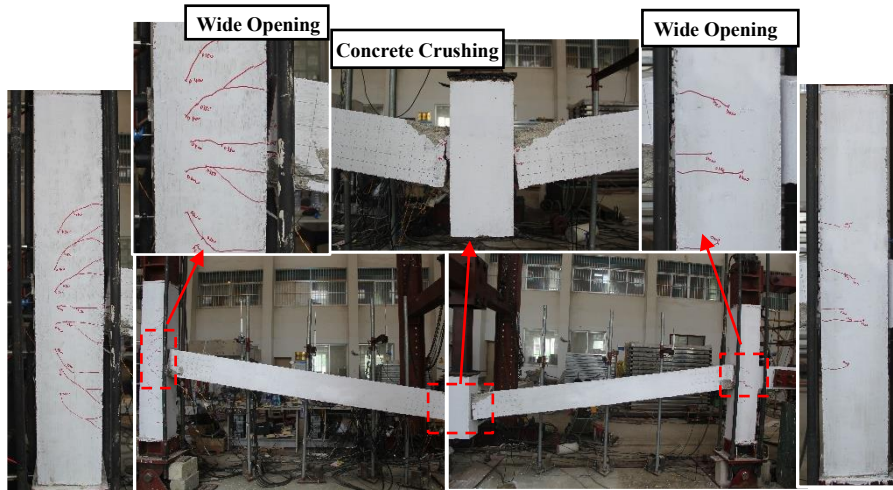


Fig. 19 Crack pattern and local damage of UPCC-SL at MJD of 320 mm

828
829
830
831
832

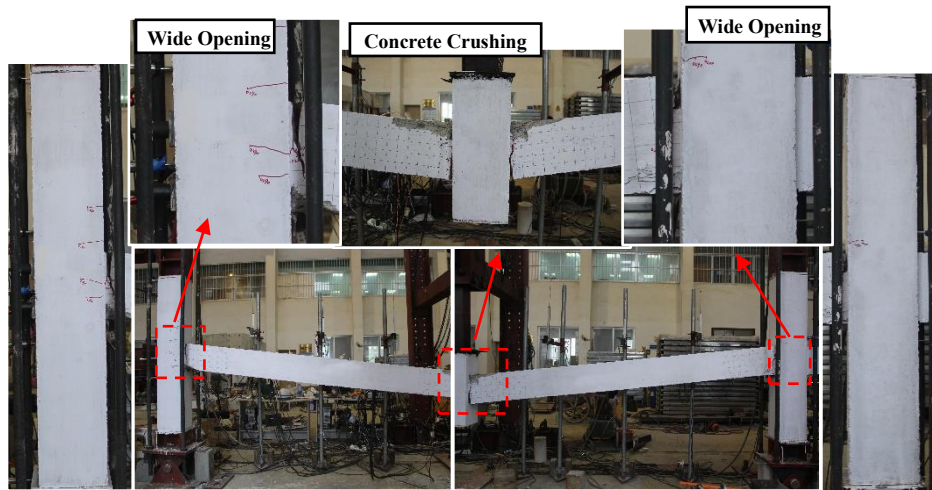


Fig. 20 Crack pattern and local damage of UPCC-SH at MJD of 295 mm

833
834
835
836
837

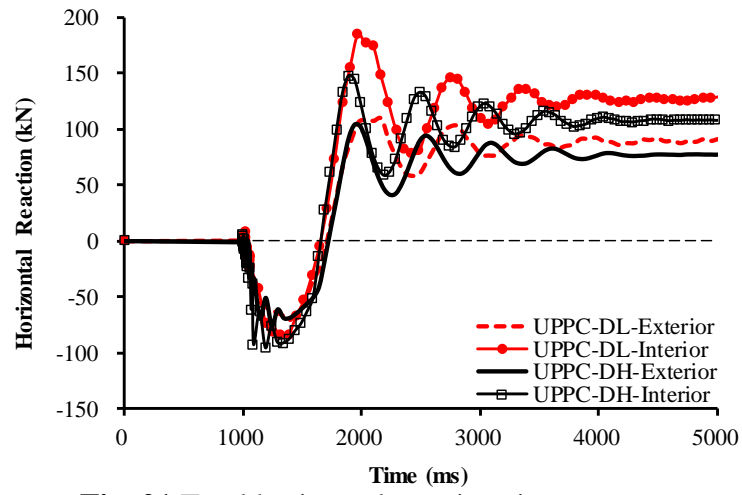


Fig. 21 Total horizontal reaction-time curves

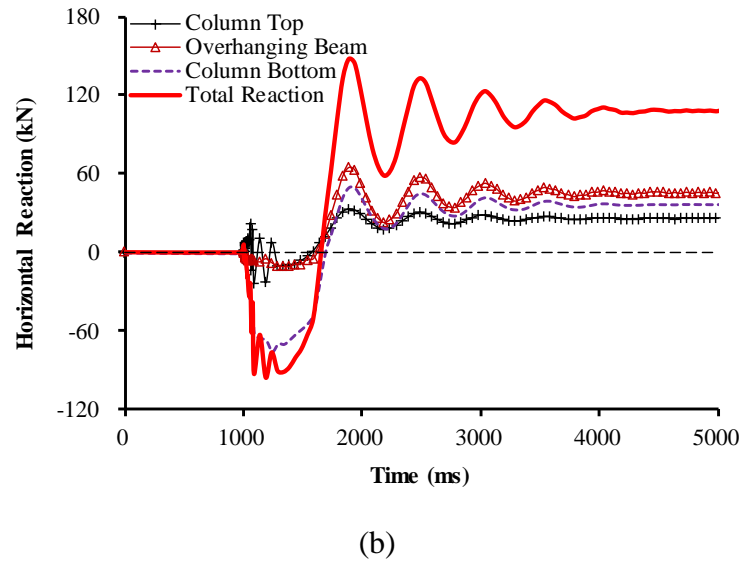
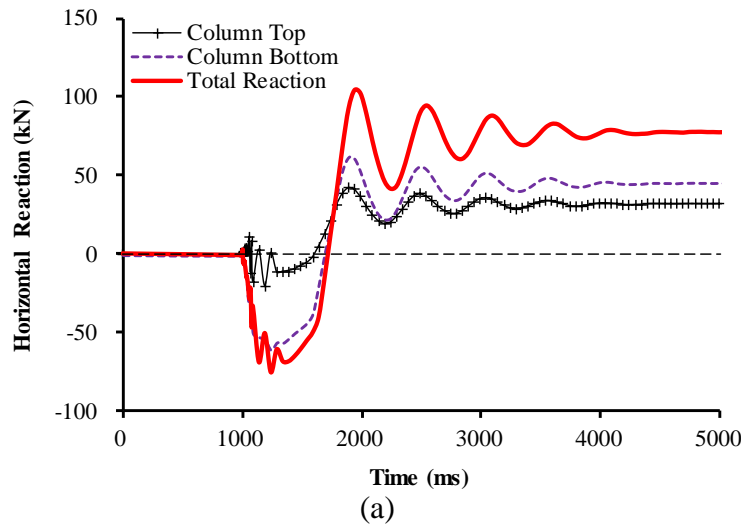
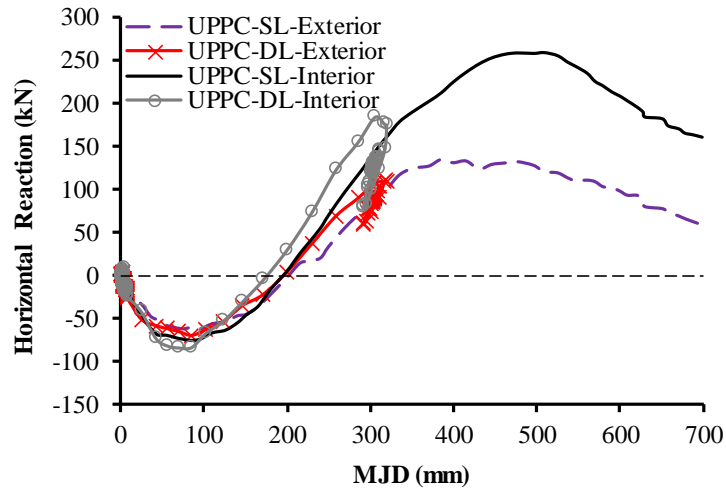


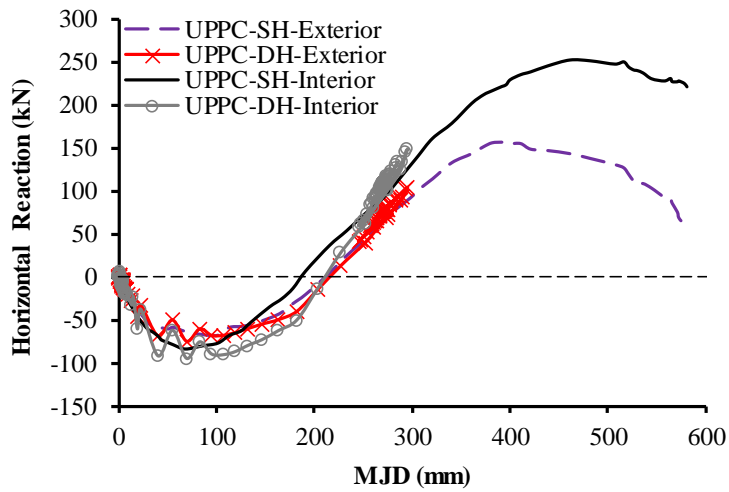
Fig. 22 Horizontal reaction of UPPC-DH: (a) exterior side; (b) interior side

855
856



(a)

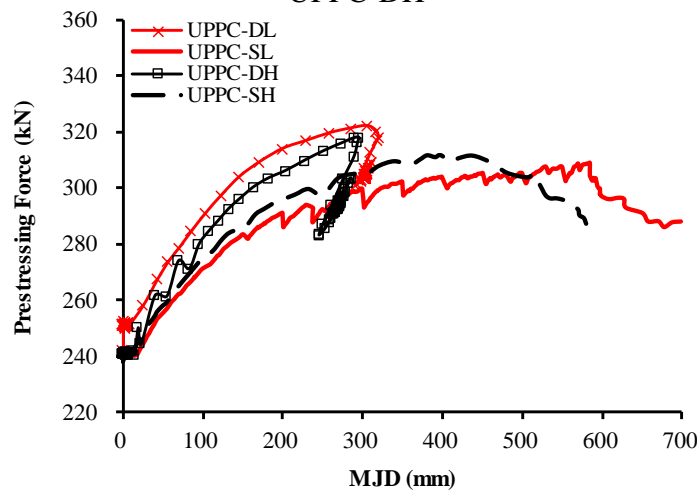
857
858
859
860



(b)

861
862
863
864
865

Fig. 23 Comparison of the total horizontal reaction: (a) UPPC-SL vs. UPPC-DL; (b) UPPC-SH vs. UPPC-DH



866
867
868
869

Fig. 24 Variation of prestressing forces in strands

870
871
872
873
874

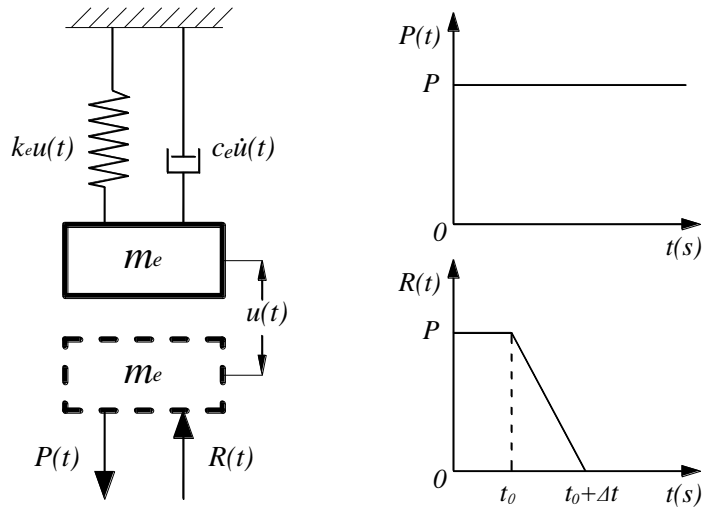
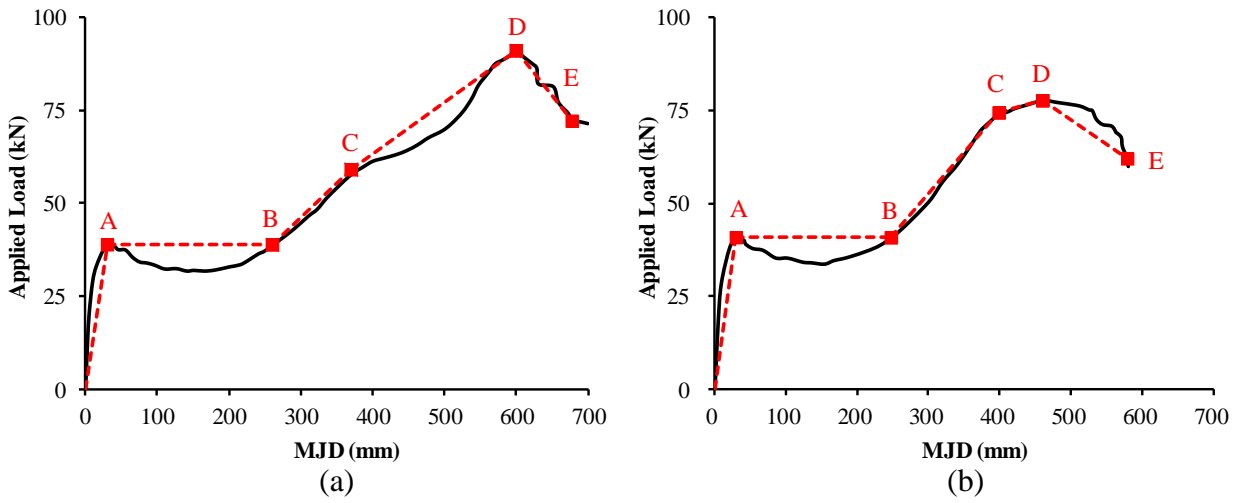
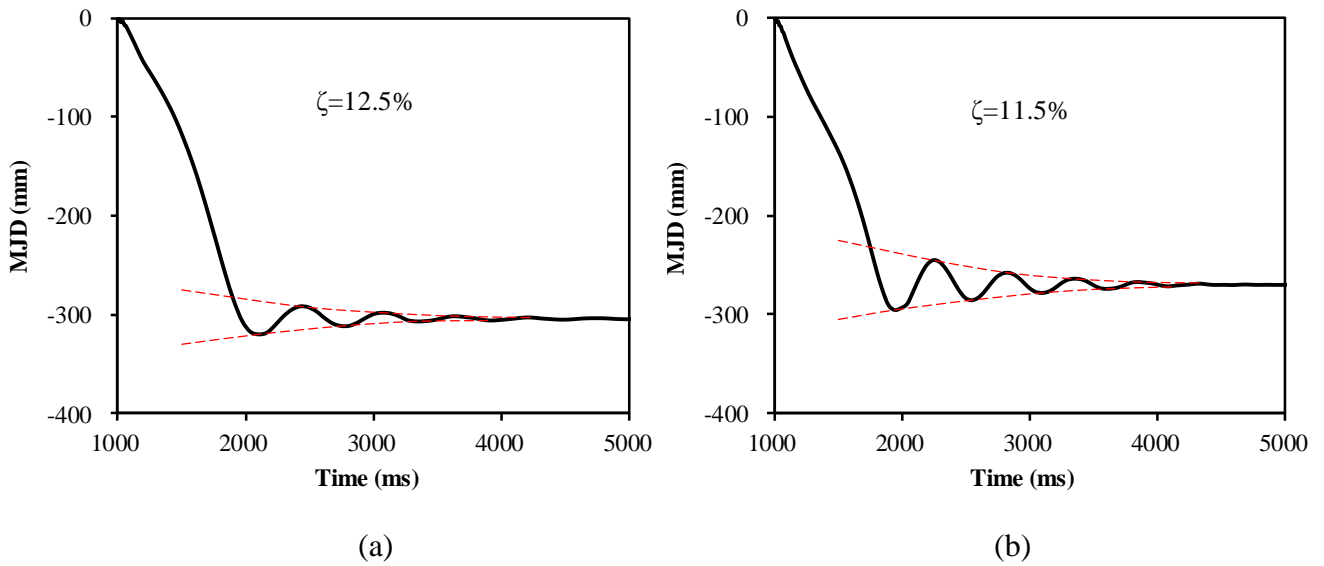


Fig. 25 Simplified SDOF model



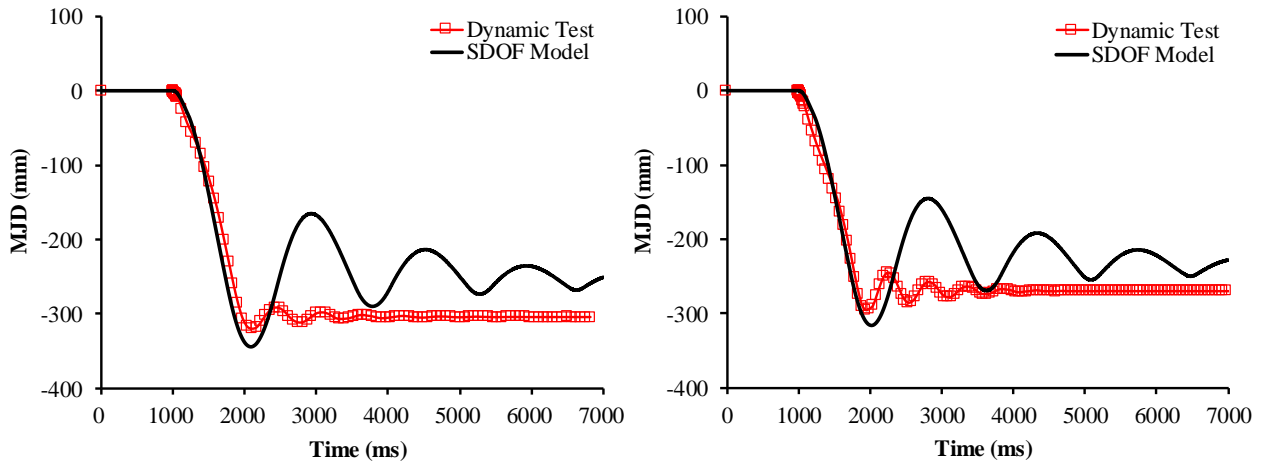
875
876
877
878
879

Fig. 26 Load resisting function: (a) UPPC-SL; (b) UPPC-SH



880
881
882
883
884
885
886

Fig. 27 Determination of damping ratio: (a) UPPC-DL; (b) UPPC-DH



(a)

(b)

Fig. 28 Comparison of the theoretical MJD to the measured one: (a) UPPC-DL; (b) UPPC-DH

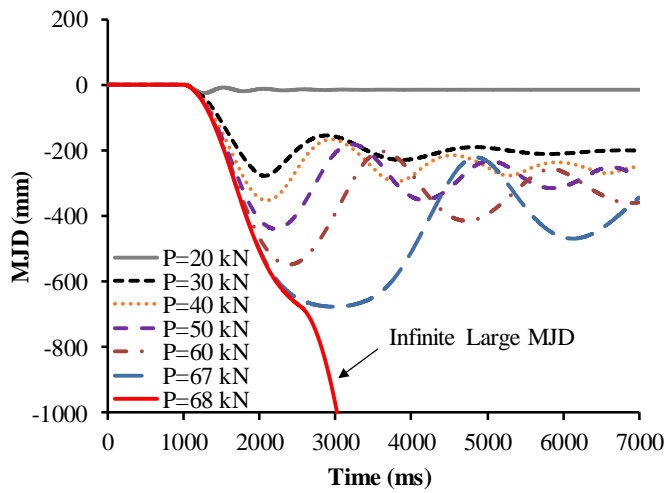


Fig. 29 Determination of dynamic ultimate load

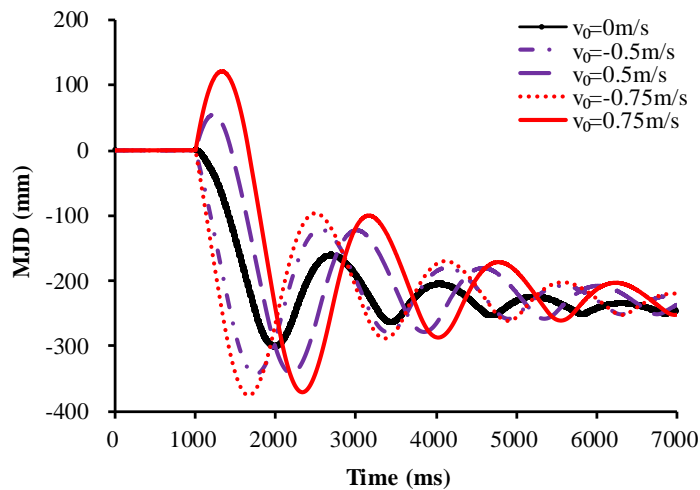


Fig. 30 Effect of initial velocity

887
888
889
890
891
892

893
894
895
896
897

898
899
900
901
902
903

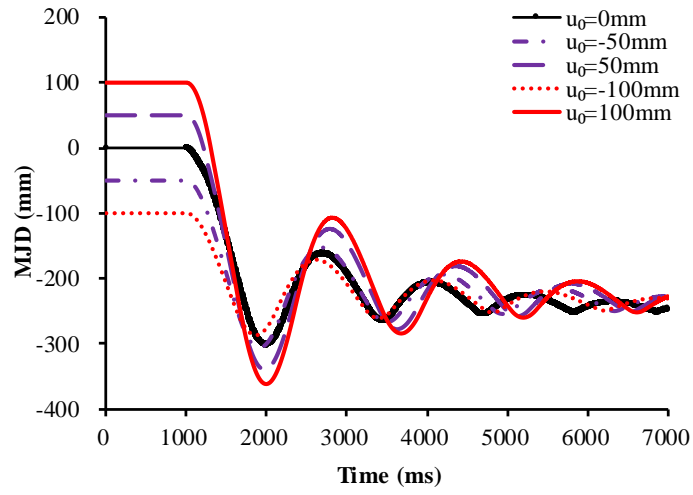


Fig. 31 Effect of initial displacement

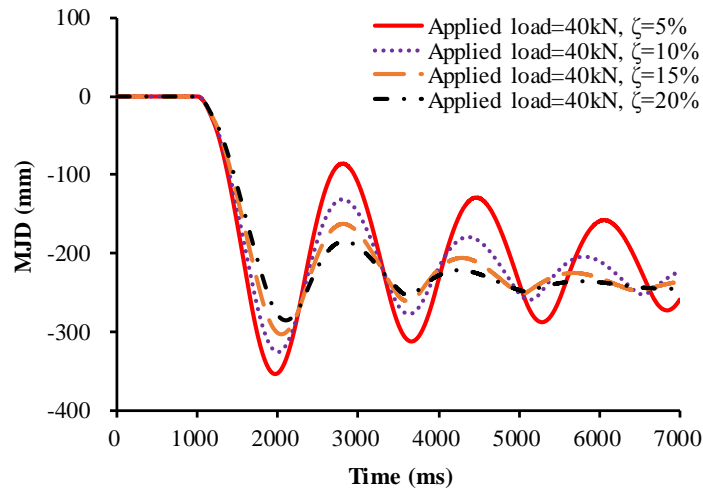


Fig. 32 Effect of damping ratio

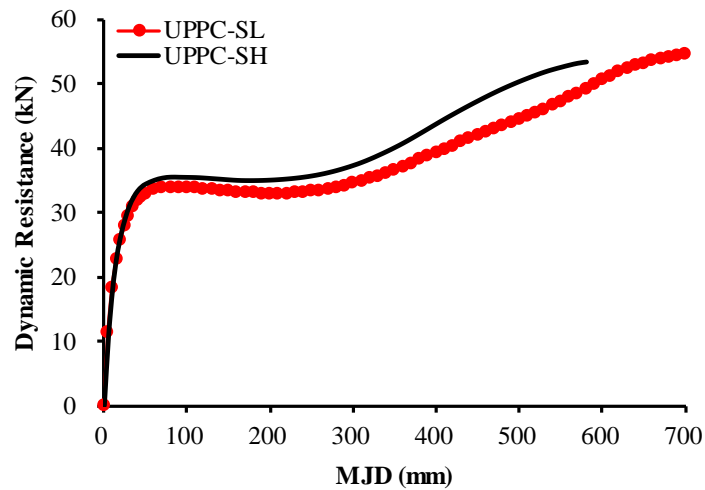


Fig. 33 Dynamic resistance based on energy method

904
905
906
907
908
909

910
911
912
913

914
915
916
917
918